Journal of Paleolithic Archaeology (2026) 9:19
https://doi.org/10.1007/s41982-026-00260-7

RESEARCH

The Middle Palaeolithic of the Pindos Range and its Neighbouring Areas: New Evidence from SMR1 (Samarina, western Macedonia, Greece)

Jacopo Gennai[1] · Paolo Biagi[2] · Maria Ntinou[3] · Elisabetta Starnini[1,4] · Nikos Efstratiou[3]

Received: 24 September 2025 / Accepted: 5 March 2026

Abstract
The Middle Palaeolithic record of the southern Balkans is largely known from open-air surface scatters that are often difficult or impossible to date and lack a clear stratigraphic context. In the area close to the Pindos range, only two sites—Theopetra cave and Asprochaliko rockshelter—yielded stratified Middle Palaeolithic deposits, while Kokkinopilos presents partial stratification, although artefacts from older excavations remain difficult to contextualise. Information on surface scatters is generally limited to typological assessments, with little insight into depositional processes or spatial distribution. SMR1 (Samarina, western Macedonia) represents an exceptionally large Middle Palaeolithic assemblage recovered from erosional patches. The site is on a terrace overlooking the Samariniotikos River located at 1517 m a.s.l. While most artefacts were found in a horizontal position on the surface, a few of them were embedded in the soil profile, suggesting a buried context affected by recent erosion and accumulation. The assemblage includes all stages of lithic reduction, from core preparation to micro-debitage, reinforcing its technological coherence and Middle Palaeolithic attribution. Despite the absence of any direct radiometric dating, the techno-typological characteristics of SMR1 can be compared with some dated and undated assemblages from the Pindos range, providing valuable evidence for the Balkan Peninsula Middle Palaeolithic debate and Neanderthal occupation of the Pindos highlands.

Keywords Greece · Pindos · Neanderthal · Middle Palaeolithic · Mousterian · Levallois

Introduction

The Middle Palaeolithic Record in the southern Balkans

The Balkan Peninsula is a crossroad and land bridge between southwestern Asia, Anatolia, and western Europe. As such, it has the potential to detect bio-cultural changes that occurred during the Pleistocene (Harvati & Roksandic, 2016; Mihailović, 2020; Mihailović et al., 2022). Renewed efforts in the northern Balkans uncovered new stratified sites attributed to the Middle and Late Pleistocene, especially adding evidence about the start and the development of the Middle Palaeolithic (Alex et al., 2019; Dogandžić, 2023; Karavanić & Banda, 2023; Mihailović, 2008, 2014; Mihailović & Whallon, 2017; Monnier et al., 2020; Stojanovski et al., 2025; Vujević & Perhoč, 2024). Similarly, research projects in continental and peninsular Greece provided new stratified sites attributed to the late Middle

✉ Elisabetta Starnini
elisabetta.starnini@unica.it

1 Department of Civilisations and Forms of Knowledge, Pisa University, Via dei Mille, 19, Pisa I-56126, Italy

2 Department of Asian and North African Studies, Ca' Foscari University, Ca' Cappello, San Polo 2035, Venezia I-30125, Italy

3 School of History and Archaeology, Aristotle University of Thessaloniki, University Campus, Thessaloniki GR-54124, Greece

4 Department of Literature, Languages and Cultural Heritage, Cagliari University, Cittadella dei Musei "Giovanni Lilliu", Piazza Arsenale 1, Cagliari I-09124, Italy

Published online: 13 April 2026

Palaeolithic (Garefalakis et al., 2018; Tourloukis et al., 2016) and the evidence of a possible complex palaeoanthropological configuration within the early Middle Palaeolithic of the southern Balkans (Falguères et al., 2025; Harvati et al., 2019; Mihailović et al., 2022). The new U/Th dates of the calcite on the Petralona cranium (286 ± 9 ka BP) provide evidence of persistence of a *Homo* species without Neanderthal or *s*apiens derivative traits (Falguères et al., 2025). This latter result is in accordance with the Mala Balanica human remains (238 + 33/−30 ka), while Velika Balanica remains (285 ± 34 ka and 295 ± 74 ka) are indicative of a Neanderthal-related population (Mihailović et al., 2022). Additionally, two crania from Apidima cave, dated to about 170 ka and 210 ka, revealed contrasting features: while the younger one shows derived Neanderthal features, hence aligning this part of Europe with the rest of the European continent, the latter has morphometric features consistent with a *Homo sapiens* attribution (Harvati et al., 2019). Therefore, the southern Balkan Peninsula could be one of the areas for an early *Homo sapiens* dispersal, as indicated by gene flow (Posth et al., 2017) and new paleoanthropological evidence from the Levant (Hershkovitz et al., 2018). In the central part of the Balkan Peninsula, represented by the Pindos mountain chain running north–south, recent investigations contributed to the recontextualization of the open-air site of Kokkinopilos, a buried context dating to the Middle Pleistocene (Tourloukis, 2010; Tourloukis et al., 2015). New research in Epirus and the Ionian islands have revealed open-air surface and reworked buried contexts with Middle Palaeolithic artefacts (Galanidou et al. 2016a, 2020, 2022; Ligkovanlis 2017; Ligkovanlis et al. 2022; Ligkovanlis and Kourtessi-Philippakis 2022; van Wijngaarden et al. 2017). Furthermore, new research in southern Albania uncovered the first stratified Middle Palaeolithic artefacts of the country (Badino et al., 2025; Ruka et al., 2025). Finally, a long-term survey project, carried out jointly by Thessaloniki Aristotle and Venice Ca' Foscari universities, identifying several findspots with Middle Palaeolithic artefacts in the mountain ridges and valleys around the town of Samarina (Grevena, Western Macedonia, Greece; Biagi et al., 2015, 2017, 2022; Efstratiou et al., 2006, 2011) have revealed an unexpected and intensive exploitation of a high-altitude environment by Neanderthal groups. High-altitude occupation during the Middle Palaeolithic is recorded in various mountain ranges in Eurasia. In Iberia, several sites are recorded within 700–1400 m a.s.l., and data suggest an occupation mostly during the warmer periods of Marine Isotope Stage (MIS) 5 and 3 (Domingo et al., 2017). Evidence from the Alps and subalpine ranges is sparse (Bona et al., 2007; Jéquier, 1975; Margaritora et al., 2020; Tillet, 2003). In the central Apennines, between 1000 and 2000 m a.s.l., surface finds have been interpreted as seasonal occupations (Radmilli, 1965). The record from the Caucasus yields more consistent data about Middle Palaeolithic high-altitude occupations (Doronicheva et al., 2024; Gasparyan et al., 2014; Malinsky-Buller et al., 2021).

The Problem of Open-air Surface Scatters

A survey of the available literature shows that the sites in the Pindos areas consist mainly of surface findspots with only a few buried contexts and even fewer dated sites (Fig. 1, SI_file 1 and references therein).

These surface lithic concentrations are the results of several survey projects (Ammerman et al. 1999; Biagi et al. 2022; Dakaris et al. 1964; Elefanti and Marshall 2015; Forsén et al. 2016; Francis et al. 2005; Galanidou 2014; Galanidou & Papoulia 2016; Galanidou et al. 2016a; Harrold et al. 1999; Harvati et al. 2008; Hauck et al. 2017; Higgs & Vita-Finzi 1966; Papoulia 2011; Ruka, 2023; Runnels, 1988; Runnels et al., 2004, 2010; Runnels & van Andel, 2003; Tourloukis & Harvati, 2018; van Andel & Runnels, 2005; van Wjingaarden et al., 2013). While they are precious evidence of Middle Palaeolithic presence in the area, none of these scatters, except for Kokkinopilos (but see the discussion), can be attributed to a precise timespan with the support of a radiometric date; hence, relative chronology is attributed to the finds on the grounds of techno-typological criteria. This approach is rather dependent on the total number of artefacts, on those retained as diagnostic, and, ultimately, the techno-typological experience and approach of the analyst (Ligkovanlis, 2017).

Aim of the Analysis

Here we present a full techno-typological analysis of SMR1, a large surface lithic concentration located in the Pindos highland zone in northwestern Macedonia (Greece). The site was discovered and investigated during the Thessaloniki-Venice Universities' Grevena Project. The unique feature of this concentration is its high number of knapped artefacts, all diagnostic of Middle Palaeolithic reduction methods. The lithic artefacts were found in a horizontal position with a complete representation of the reduction steps.

The main aim is to provide a full description of SMR1 technical behaviour. Furthermore, this effort lays the groundwork for discussion and comparison with lithic evidence attributed to the Middle Palaeolithic from surface concentrations and buried sites in the neighbouring region to elucidate technological behaviours in likely related areas.

Materials and Methods

The SMR1 Site

The site was discovered by team member, Ploutarchos Mitsakos, during a survey conducted around the village of Samarina in October 2010. The site is located at 1517 m a.s.l. on a higher terrace overlooking the Samariniotikos River, approximately 3.5 km upstream from Samarina (Biagi et al., 2017; Figs. 1 and 2).

It is characterised by three areas of collection that correspond to the three erosional patches: SMR-1W, SMR-1 (central) and SMR-1E. SMR-1W partially corresponds to a modern lateral slope, while SMR-1E is on the frontal slope. The Samariniotikos River, forming a sharp bend separates SMR1 from the SMR-2 findspot (Fig. 3). The artefacts from the two findspots are very similar in raw materials used, technology, and typology (Biagi et al., 2017). Most probably, the site extends under the grass cover in the areas adjacent to the erosion. Future excavations might reveal the original extension of the site that was certainly larger than the part exposed by the erosional patches.

Artefacts at SMR1 were collected using a 10 cm square grid, and the spatial coordinates of each piece were recorded on the square grid. The surface collection was repeated for two survey seasons. Two test pits were excavated to investigate sedimentary contexts by Diego Ercole Angelucci, one at the upper boundary of the SMR-1 central erosional patch (square K15: Fig. 4) and another adjacent to the SMR-1W erosional patch (square F23: Fig. 4). Few artefacts were recovered during the excavation of the geological profiles. The F23 test pit (50 × 50 cm, surface height 457 cm above datum point: see Fig 27 in Biagi et al., 2017) consists of five main stratigraphic units. U1 is a modern, poorly developed

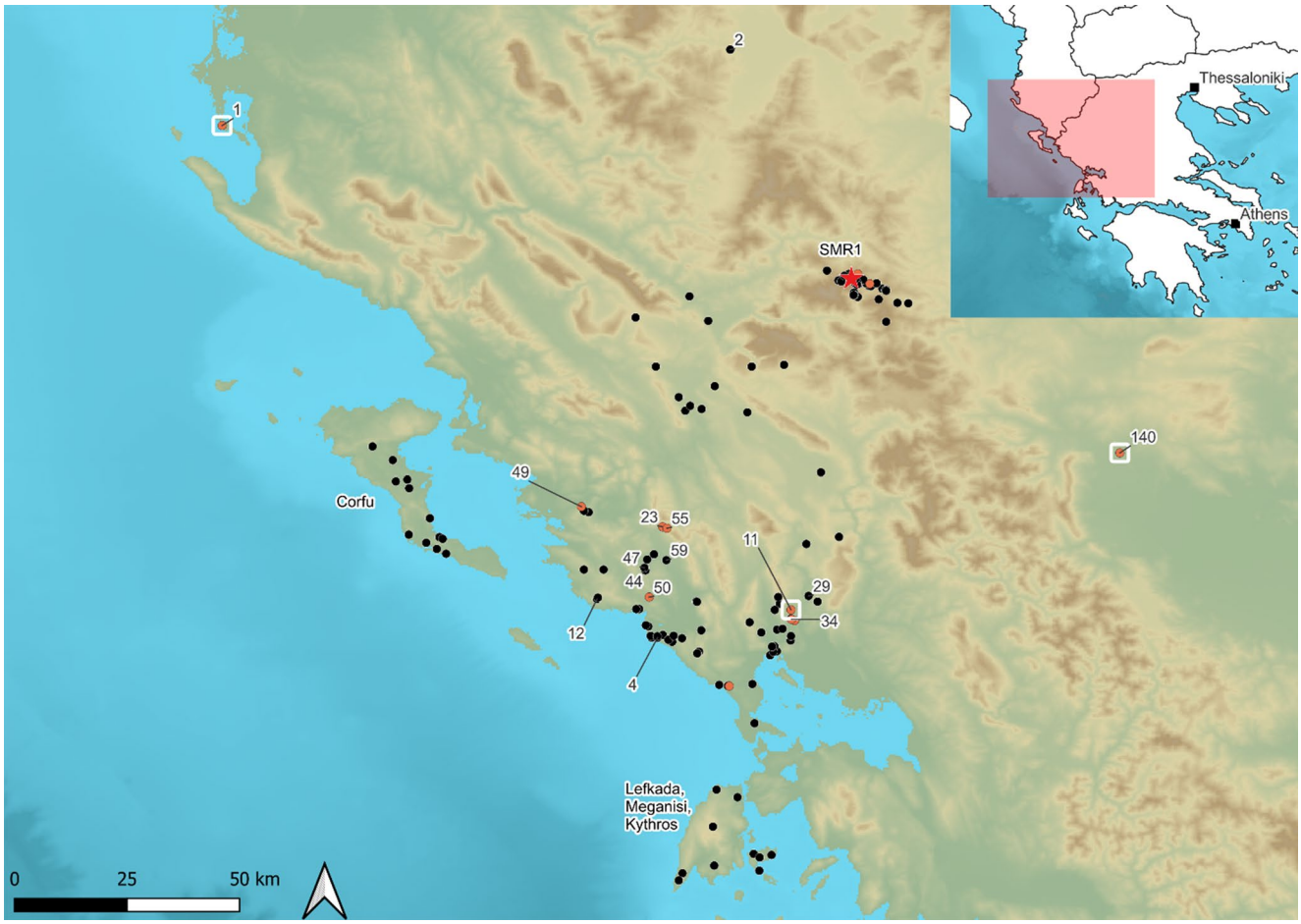

Fig. 1 Map of the central Pindos area sites yielding Middle Palaeolithic artefacts. Orange circles represent sites with artefacts in buried contexts, while the black circles are surface scatters, and white squares are radiometrically dated sites. Sites mentioned in the text:1–Dalani i Vogël, 2–Istrahista, 4–Alonaki, 11–Asprochaliko rockshelter, 12–Agia, 23–Eleftherochori 7, 29–Gortses, 34–Kokkinopilos, 44–Megalo Karvounari, 47–Mikro Karvounari, 49–Molondra, 50–Morfi, 55–Popovo, 59–PS 43, 140–Theopetra Cave, Corfu and the Lefkada-Maganisi-Kithros complex. Both maps have been elaborated in QGIS 3.36 Maidenhead (Jacopo Gennai), elevation data elaborated from the GEBCO_Grid 2023 (GEBCO Bathymetric Compilation Group, 2023, 2023), a full list and coordinates of the sites is available in the SIFile_1 of the manuscript

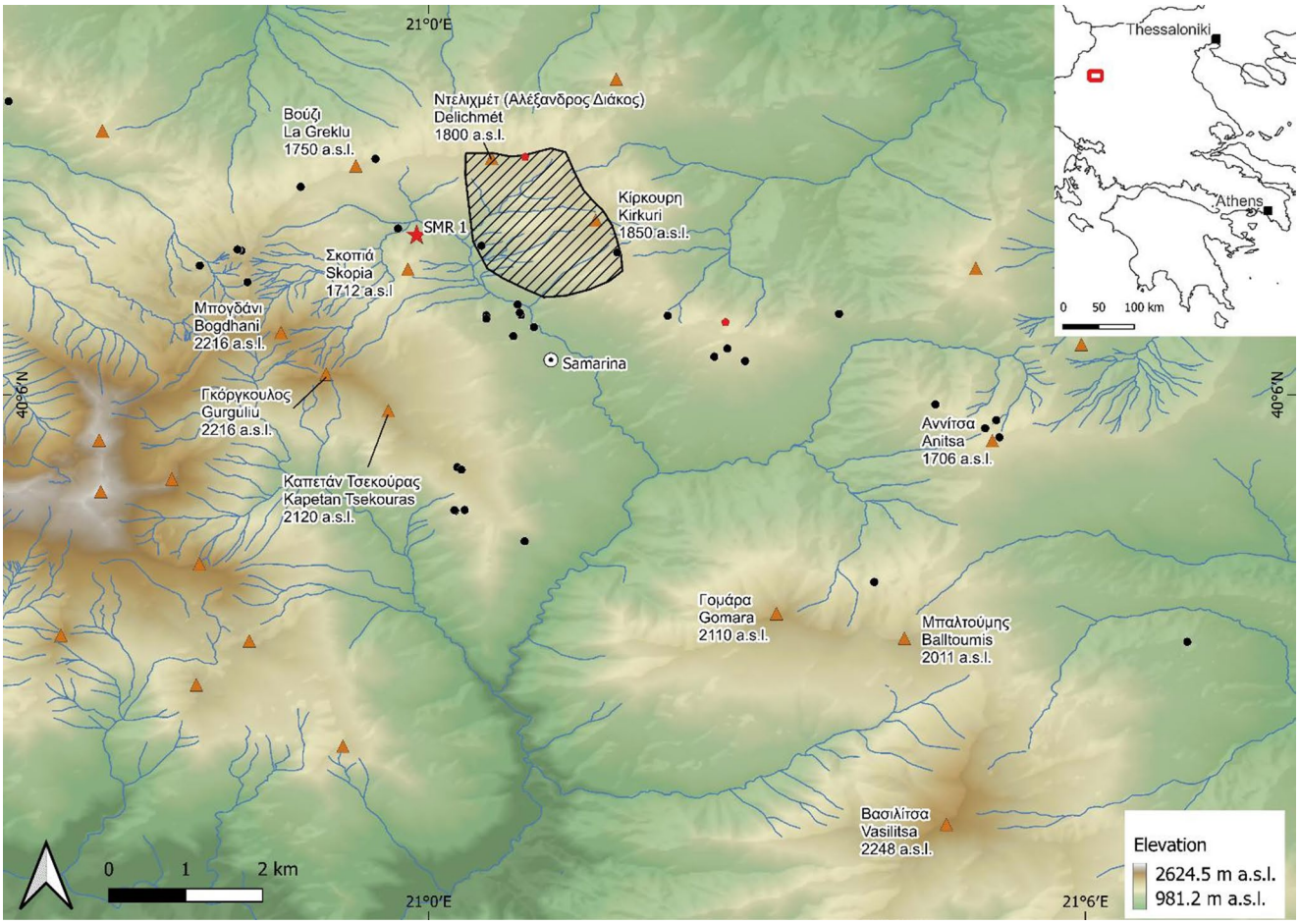

Fig. 2 Topographical map of the Samarina highlands with some of the Middle Palaeolithic findspots (black dots and red pentagons), mountain peaks (orange triangles), the location of SMR1 (red star), and Samarina modern town (white circle with black middle dot). Top right corner, the location (red rectangle) of the represented area within Greece. The striped area corresponds to the raw material outcrops (Biagi et al., 2015). The map has been elaborated in QGIS 3.36 Maidenhead (Jacopo Gennai), elevation data produced using Copernicus WorldDEM-30 © DLR e.V. 2010–2014 and © Airbus Defence and Space GmbH 2014–2018 provided under COPERNICUS by the European Union and ESA; all rights reserved

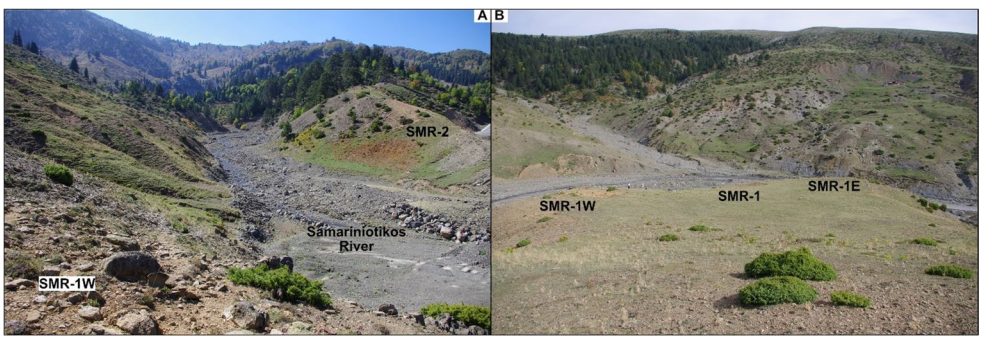

Fig. 3 Location of SMR1 and 2 findspots. (**a**) The Samariniotikos River separating SMR-2 (right) from SMR1 (on the left). (**b**) SMR1 findspots with the location of the three erosional patches (from left to right −1W, −1, and −1E). In front, the Samariniotikos River and the chert outcrops area. (Photographs by Paolo Biagi 2014)

A horizon (457–452 cm) of silty loam with scarce stones and organic matter. U2 (452–430 cm) is an AC horizon of almost pure silt, low in organics, with a concentration of stones and an artefact at its base. U3 (430–407 cm), a 2 C horizon, comprises silt with some clay and scattered sandstone fragments, containing abundant microcharcoal. U4 (407–395 cm), a dense 3B horizon, and U5 (395–385 + cm), a mottled 3Bg horizon with Mn nodules, are interpreted as part of a truncated Pleistocene paleosol formed on fine alluvial sediments. No carbonates were found in any unit. Artefacts from F23 include a chert chip from U1, a large flake at the U2/U3 boundary (oriented N–S), and two small chips from the top of U4; charcoal fragments were also collected for identification and radiocarbon dating (Biagi et al., 2022).

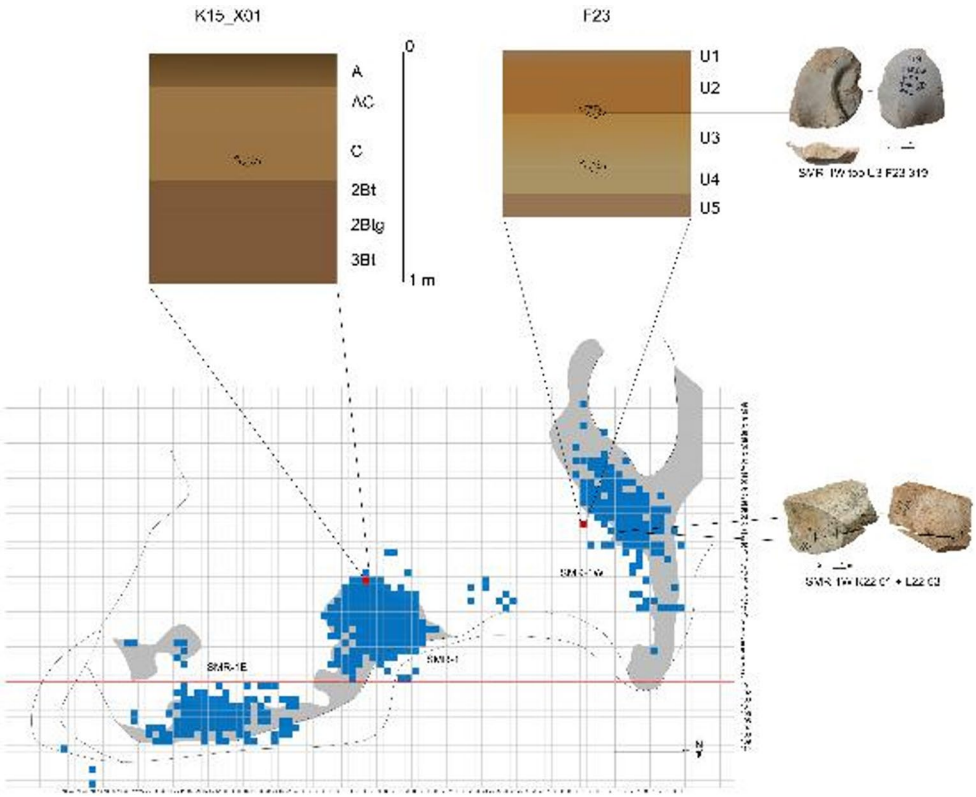

Fig. 4 The grid used for the collection of artefacts is superimposed on the SMR1 terrace morphology. Blue squares indicate areas of artefact collection, while shaded grey areas represent erosional patches. Red squares denote the locations of test pits. On top, the test pit profile sketches and the location of artefact retrieval, as well as the artefact recovered at the interface between U2 and U3 in the F23 test pit. On the right, SMR-1W K22 51 + L22 53 artefact conjoin. (Drawings by Jacopo Gennai, photographs by Elisabetta Starnini)

In K15 (197 cm above datum point), the stratigraphy comprises a modern soil sequence overlying a lithological discontinuity marking the context of Middle Palaeolithic finds. The A horizon (0–15 cm) is silty loam with few sandstone fragments and low porosity. Below this, the AC (15–35 cm) and C horizons (35–55 cm) continue the silty texture, with increasing stone content and almost no organic matter. Beneath the discontinuity, the buried paleosol begins with a 2B(t) horizon (55–70 cm) of clayey silt with faint Fe/Mn mottles and thin coatings, followed by a 2Btg horizon (70–80/90 cm) with scarce stones, stronger mottling, nodules, and slight cementation. The 3Bt horizon (80/90–100 + cm), not fully excavated, is silty clay with frequent coatings and no stones.

A total of 1819 artefacts were recovered. The majority derive from the central recovery area (SMR-1; $n = 1082$), followed by SMR-1W ($n = 461$) and SMR-1E ($n = 271$). An additional five artefacts were recovered from the cleaning of the profiles. The maximum artefact density is recorded in square O10 ($N = 32$, SITable 1), and the median number of artefacts is four by square metre in SMR-1, two in SMR-1W, and one in SMR-1E.

The artefacts have been found mostly lying horizontally on the ground, and more artefacts are eroding from the soil profile (Fig. 5).

Techno-typological Approach

The SMR1 assemblage has been studied during two study seasons, each three weeks long. During the first stay, only complete blanks and cores were selected, while the rest of the assemblage was recorded in the second stay.

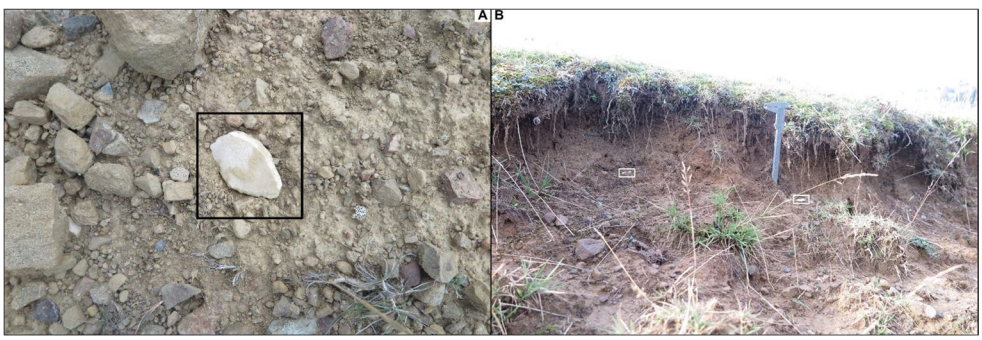

Fig. 5 In situ artefacts of SMR1. (**a**) Middle Palaeolithic sidescraper lying horizontally on the ground in 2024 (black rectangle). (**b**) Middle Palaeolithic artefacts (white rectangles) buried in the soil profile at the upper border of the SMR-1 erosional patch in 2024. (Photographs by Jacopo Gennai)

The *chaîne opératoire* approach (Soressi & Geneste, 2011) and the most common criteria recognised for the main Middle Palaeolithic methods have been employed: Levallois (Boëda, 1994; Guette, 2002), Discoid (Boëda, 1993; Peresani, 2003), Orthogonal (Forestier, 1993), Volumetric (Carmignani & Soressi, 2023). Additionally, the attribute analysis put forward by Bustos-Pérez and colleagues (2023) has been followed. Those attributes were designed to investigate the robustness of attributes in differentiating between discoid and Levallois methods (Bustos-Pérez et al., 2023). In particular, Bustos-Pérez and colleagues (2023) concluded that the internal platform angle (IPA), the external platform angle (EPA), and the mean thickness were the most useful attributes in differentiating Levallois, discoid, and hierarchical discoid knapping products.

Therefore, after a cross-evaluation of the assemblage and the division of the artefacts into major categories (cores, cortical blanks, predetermining blanks, predetermining and predetermined blanks, target blanks), each artefact was recorded individually in a digital database. The databases are shared as Supplementary Information attached to the manuscript, and they are intended to provide quantitative, reusable, and interoperable raw data (SIFile_2, SIFile_3, SIFile_4).

The recorded attributes are numerical (flaking angle, length, width, thickness, platform dimensions) and categorical (presence and location of cortical surface, platform type, presence of lipping, presence of bulbar scar, overhang microchipping, scar pattern, technological category, place of the artefact in the reduction, morpho-technological attributes, taphonomic observations, presence of retouch and retouch descriptive attributes).

All the dimensions are recorded manually with a digital calliper with a maximum instrumental error of 0.02 mm and a resolution of 0.01 mm. Recordings are automatically input thanks to a data cable.

Statistical differences were assessed using the Chi-squared test for qualitative (categorical) variables and the Kruskal-Wallis non-parametric test for numerical variables. All statistical testing is performed into the open-source software R version 4.5.2 (R Core Team, 2025), using the ggstatsplot package (Patil, 2021).

Retouch analysis and description followed Inizan et al.'s attributes (1999), and typological classification followed Laplace's (1964) and F. Bordes's proposals (1961, 1988).

Results

In the following section, the lithic technological analysis of SMR1 patches will be presented. The excavated sample (SMR1-exc) will be left out of statistical testing due to the small size.

General Composition of the Assemblages

In all the collection areas, flakes are the most abundant category, followed by undetermined fragments (Table 1). A chi-square test of independence was performed to evaluate whether the frequencies of artefact categories differ across the sites. The result is highly significant ($\chi^2 = 42.8$, df = 8, p = < 0.001), indicating that the distribution of categories is not uniform across sites. However, the effect size is small (Cramer's V = 0.098), suggesting that the differences, while statistically significant, are subtle. The largest deviations from expected frequencies occur in flakes and debris, with SMR-1 having a relatively higher percentage of undetermined fragments and a slightly lower percentage of flakes, whereas SMR-1W shows the opposite pattern. Cores and laminar items are more evenly distributed across sites, with only minor deviations that do not reach statistical significance.

Taphonomy

The artefacts show fresh ridges and mostly fresh edges (Table 2), although there is some extent of edge damage and evidence of lichen patina but no double patina that would indicate a recent damage. A chi-square test of independence was performed to evaluate whether the frequencies of edge damage differ across the sites. The result is highly significant ($\chi^2 = 98.73$, df = 2, p = < 0.001), indicating that the distribution of edge damage is not uniform across sites. The effect size is medium (Cramer's V = 0.231). Edge damage is mostly found in SMR-1W and SMR-1E, while it is negligible in SMR-1. The degree of fragmentation is similar for laminar items and cores across the three main assemblages, while a statistical difference arises in flakes ($\chi^2 = 66.9$, df = 12, $p < 0.001$, Cramer's V = 0.145). The main difference lies in frequencies of complete flake blanks, which is higher in SMR-1W ($N = 176$, 47.7%; Table 1), while complete flake blanks in SMR-1 account for a third of the total ($N = 247$, 33.1%; Table 1).

Technology

The assemblages feature all elements of the *chaîne opératoire* (Table 3). Volumetric blades and bladelets are extremely rare; the majority of blade and bladelet-like blanks are elongated versions of technological categories found in flakes.

Cores

Levallois cores are the most frequent across the three assemblages, followed by hierarchical discoid ones (Table 3, Fig. 6). Two prismatic cores have been found in SMR-1E and SMR-1W, respectively (Table 3). The cortical presence is

Table 1 Assemblage composition and degree of fragmentation of the various categories. Percentages represent frequency along the same row except for the total columns where percentages refer to frequency of the debitage product within the subtotal

Categories	SMR-1		SMR-1E		SMR-1W		SMR1-exc		Total	
	N	%	*N*	%	*N*	%	*N*	%	*N*	%
Blade	**53**	**4.9**	**17**	**5.6**	**21**	**4.5**		**0.0**	**91**	**4.9**
Whole	33	62.3	12	73.3	12	55.0			57	62.5
Proximal + Mesial	12	22.6	3	13.3	4	20.0			19	20.5
Mesial	4	7.5	1	6.7	1	5.0			6	6.8
Mesial + Distal	4	7.5	1	6.7	3	15.0			8	9.1
Incomplete		0.0		0.0	1	5.0			1	1.1
Bladelet	**9**	**0.8**	**3**	**1.1**	**2**	**0.5**		**0.0**	**14**	**0.8**
Whole	2	22.2	1	33.3		0.0			3	21.4
Proximal + Mesial	5	55.6	1	33.3	2	100.0			8	57.1
Mesial	2	22.2	1	33.3		0.0			3	21.4
Core	**18**	**1.7**	**13**	**4.5**	**16**	**3.2**		**0.0**	**47**	**2.4**
Whole	12	66.7	10	75.0	10	57.1			32	65.9
Incomplete	6	33.3	3	25.0	6	42.9			15	34.1
Flake	**746**	**68.9**	**196**	**73.0**	**367**	**79.9**	**4**	**80.0**	**1313**	**72.3**
Whole	247	33.1	74	37.4	176	47.7	1	25.0	498	37.7
Proximal	64	8.6	13	6.7	29	8.2		0.0	106	8.2
Proximal + Mesial	64	8.6	29	14.9	38	9.9	1	25.0	132	9.9
Mesial	40	5.4	11	5.6	29	7.9		0.0	80	6.1
Mesial + Distal	28	3.8	11	5.6	20	5.6		0.0	59	4.5
Distal	44	5.9	4	2.1	22	6.2	1	25.0	71	5.5
Incomplete	259	34.7	54	27.7	53	14.4	1	25.0	367	28.1
Fragment	**256**	**23.7**	**42**	**15.7**	**55**	**12.0**	**1**	**20.0**	**354**	**19.6**
Total	**1082**	**100.0**	**271**	**100.0**	**461**	**100.0**	**5**	**100.0**	**1819**	**100.0**

Table 2 Presence of mechanical edge damage across the collection areas and the artefact categories

Categories	No		Yes		Total	
	N	%	*N*	%	*N*	%
SMR-1	953	88.1	129	11.9	1082	100.0
Blade	29	54.7	24	45.3	53	100.0
Bladelet	9	100.0		0.0	9	100.0
Core	18	100.0		0.0	18	100.0
Flake	642	86.1	104	13.9	746	100.0
Fragment	255	99.6	1	0.4	256	100.0
SMR-1E	**197**	**72.3**	**74**	**27.7**	**271**	**100.0**
Blade	9	46.7	8	53.3	17	100.0
Bladelet	3	100.0		0.0	3	100.0
Core	13	100.0		0.0	13	100.0
Flake	130	66.2	66	33.8	196	100.0
Fragment	42	100.0		0.0	42	100.0
SMR-1W	**312**	**67.5**	**149**	**32.5**	**461**	**100.0**
Blade	11	50.0	10	50.0	21	100.0
Bladelet	2	100.0		0.0	2	100.0
Core	16	100.0		0.0	16	100.0
Flake	231	63.0	136	37.0	367	100.0
Fragment	52	94.3	3	5.7	55	100.0
SMR1-exc	**5**	**100.0**		**0.0**	**5**	**100.0**
Flake	4	100.0		0.0	4	100.0
Fragment	1	100.0		0.0	1	100.0
Total	**1467**	**80.7**	**352**	**19.3**	**1819**	**100.0**

Table 3 Technological categories across assemblages

Technological categories	SMR-1		SMR-1E		SMR-1W		SMR1-exc		Total	
	N	%	*N*	%	*N*	%	*N*	%	*N*	%
Blade	53	4.9	17	5.6	21	4.5		0.0	91	4.9
Blade	3	5.7	1	6.7		0.0			4	4.5
Core-Edge Flake	9	17.0	8	53.3	4	15.0			21	22.7
Cortical Flake	1	1.9		0.0		0.0			1	1.1
Kombewa Flake	1	1.9		0.0	1	5.0			2	2.3
Levallois Blade	11	20.8	3	13.3	9	45.0			23	25.0
Levallois Recurrent Flake	17	32.1	4	20.0	3	15.0			24	26.1
Overshot Flake	8	15.1	1	6.7	3	15.0			12	13.6
Predetermining Flake	3	5.7		0.0	1	5.0			4	4.5
Bladelet	**9**	**0.8**	**3**	**1.1**	**2**	**0.5**		**0.0**	**14**	**0.8**
Bladelet	1	11.1	2	66.7	2	100.0			5	35.7
Levallois Recurrent Flake	2	22.2		0.0		0.0			2	14.3
Predetermining Flake	6	66.7	1	33.3		0.0			7	50.0
Core	**18**	**1.7**	**13**	**4.5**	**16**	**3.2**		**0.0**	**47**	**2.4**
Centripetal		0.0	1	8.3		0.0			1	2.3
Discoid	1	5.6		0.0	1	7.1			2	4.5
Expedient		0.0	1	8.3	2	14.3			3	6.8
Hierarchical Discoid	4	22.2	3	25.0	3	21.4			10	22.7
Levallois	11	61.1	6	50.0	9	50.0			26	54.5
Levallois and Hierarchical Discoid		0.0	1	8.3		0.0			1	2.3
Prismatic		0.0	1	0.0	1	7.1			2	2.3
SSDA	2	11.1		0.0		0.0			2	4.5
Flake	**746**	**68.9**	**196**	**73.0**	**367**	**79.9**	**4**	**80.0**	**1313**	**72.3**
Core-Edge Flake	50	6.7	17	8.2	49	13.6		0.0	116	8.8
Cortical Flake	18	2.4	13	6.7	10	2.5		0.0	41	3.1
Crest	1	0.1		0.0		0.0		0.0	1	0.1
Discoid Centripetal Flake	8	1.1	5	2.6	6	1.7		0.0	19	1.5
Discoid Core-Edge Flake	6	0.8	3	1.5	2	0.3		0.0	11	0.8
Flake	340	45.6	67	34.4	109	30.5	3	75.0	519	39.9
Kombewa Flake	92	12.3	25	12.8	21	5.6		0.0	138	10.5
Levallois Blade		0.0	1	0.5	2	0.6		0.0	3	0.2
Levallois point		0.0	1	0.5		0.0		0.0	1	0.1
Levallois Preferential Flake	4	0.5	1	0.5	8	2.3		0.0	13	1.0
Levallois Recurrent Flake	88	11.8	37	19.0	85	22.6		0.0	210	15.8
Overshot Flake	32	4.3	6	3.1	20	5.4		0.0	58	4.4
Predetermining Flake	96	12.9	17	8.7	46	12.4	1	25.0	160	12.2
Pseudo-Levallois point	11	1.5	3	1.5	9	2.5		0.0	23	1.8
Fragment	**256**	**23.7**	**42**	**15.7**	**55**	**12.0**	**1**	**20.0**	**354**	**19.6**
Total	**1082**	**100.0**	**271**	**100.0**	**461**	**100.0**	**5**	**100.0**	**1819**	**100.0**

consistently on the core face opposite to the flaking surface (base; Table 4).

Cores have mostly a single flaking surface across all the assemblages and types (SI Table 2). The scar pattern is mostly centripetal in SMR-1, while it is mostly unidirectional in SMR-1E and SMR-1W (Table 5). Most of the cores produce flakes in all the assemblages (Table 5).

The overhang microchipping is slightly more frequent in cores across all assembalges, especially in SMR-1E (SI Table 3). It is especially frequent in Levallois cores, across all assemblages (SIFile_3). Striking platforms are mostly facetted in Levallois cores, across all assemblages. Hierarchical discoid cores have mostly facetted striking platforms in SMR-1, while they are mostly plain in the other two assemblages (Table 6).

Blanks

The same blank technological categories are found throughout the different assemblages. Considering all blank categories together, simple flakes are the most frequent, followed by Levallois recurrent flakes, predetermining flakes removing ridges and blanks creating convexities (core-edge flakes, or *éclates débordantes*, overshot flakes

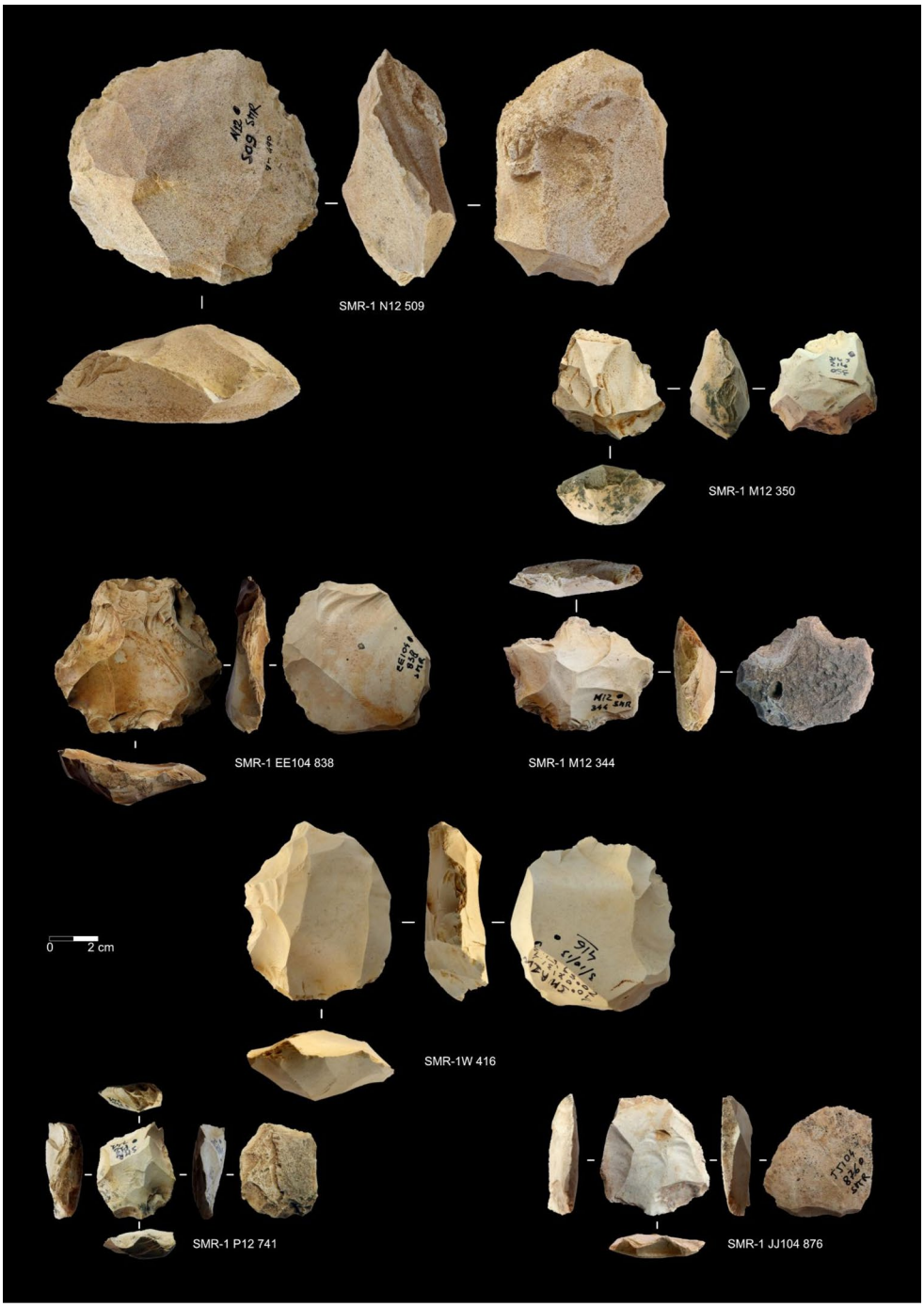

Fig. 6 SMR-1 Cores. Levallois: SMR-1 M12 350, SMR-1E EE104 838, SMR-1W 416, SMR-1 P12 741, SMR-1E JJ104 876. Hierarchical discoid cores: SMR-1 N12 509, SMR-1 M12 344. The labels correspond to the artefact ID. (Photographs by Elisabetta Starnini)

and pseudo-Levallois points), Kombewa flakes and cortical flakes (Figs. 7, 8 and 9; Table 7). A chi-square test of independence was performed to evaluate whether the frequencies of technological types differ across the assemblage. The result is highly significant (χ^2 = 92.8, df=30, p=<0.001), indicating that the distribution of technological categories is not uniform across sites. However, the effect size is small (Cramer's V=0.149). SMR-1 shows a higher frequency of simple flakes, while SMR-1E and 1W show a higher frequency of Levallois recurrent flakes and core-edge flakes (Table 7). Cortical flakes are more present in SMR-1E, and Kombewa flakes are rarer in SMR-1W.

Blanks are largely non-cortical throughout the assemblages (Table 8). Most blanks featuring cortical surfaces show less than 50% of the dorsal face covered by it. However, in SMR-1E blanks with a higher presence of cortical surfaces are more frequent, in accordance with a higher frequency of cortical flakes (Table 8). The lateral position of

Table 4 Cortex presence and location in cores across assemblages

Categories	SMR-1		SMR-1E		SMR-1W		Total	
	N	%	*N*	%	*N*	%	*N*	%
Centripetal		**0.0**	**1**	**8.3**		**0.0**	**1**	**2.3**
yes			*1*	*100.0*			*1*	*100.0*
Base			1	100.0			1	100.0
Discoid	**1**	**5.6**		**0.0**	**1**	**7.1**	**2**	**4.5**
yes	*1*	*100.0*			*1*	*100.0*	*2*	*100.0*
Base		0.0			1	100.0	1	50.0
Proximal	1	100.0				0.0	1	50.0
Expedient		**0.0**	**1**	**8.3**	**2**	**14.3**	**3**	**6.8**
no			*1*	*100.0*	*1*	*50.0*	*2*	*66.7*
yes				*0.0*	*1*	*50.0*	*1*	*33.3*
Base					1	100.0	1	100.0
Hierarchical Discoid	**4**	**22.2**	**3**	**25.0**	**3**	**21.4**	**10**	**22.7**
no	*1*	*25.0*	*3*	*100.0*	*1*	*33.3*	*5*	*50.0*
yes	*3*	*75.0*		*0.0*	*2*	*66.7*	*5*	*50.0*
Base	3	100.0			2	100.0	5	100.0
Levallois	**11**	**61.1**	**6**	**50.0**	**9**	**50.0**	**26**	**54.5**
no	*5*	*45.5*	*2*	*33.3*	*6*	*57.1*	*13*	*45.8*
yes	*6*	*54.5*	*4*	*66.7*	*3*	*42.9*	*13*	*54.2*
Base	4	66.7	3	75.0	2	66.7	9	69.2
Distal		0.0	1	25.0		0.0	1	7.7
Lateral	2	33.3		0.0		0.0	2	15.4
Proximal		0.0		0.0	1	33.3	1	7.7
Levallois and Hierarchical Discoid		**0.0**	**1**	**8.3**		**0.0**	**1**	**2.3**
no			*1*	*100.0*			*1*	*100.0*
Prismatic		**0.0**	**1**	**0.0**	**1**	**7.1**	**2**	**2.3**
yes			*1*		*1*	*100.0*	*2*	*100.0*
Base					1	100.0	1	100.0
Base and Back			1			0.0	1	0.0
SSDA	**2**	**11.1**		**0.0**		**0.0**	**2**	**4.5**
yes	*2*	*100.0*					*2*	*100.0*
Base	1	50.0					1	50.0
Lateral	1	50.0					1	50.0
Total	**18**	**100.0**	**13**	**100.0**	**16**	**100.0**	**47**	**100.0**

cortical surfaces is consistently the most frequent in semi-cortical blanks, while extensively cortical and fully cortical blanks have cortical surfaces covering much of the dorsal face. Semi-cortical blanks are mostly core-edge blanks.

Unidirectional negatives are the most frequent in blanks across all the assemblages, followed by centripetal (Table 9). Crossed negatives are the third-most frequent. Flakes are the most determined negatives in blanks across all the assemblages. While unidirectional and centripetal flakes are common in Levallois recurrent flakes, crossed negatives are mostly found in core-edge and predetermining flakes.

The proximal parts are consistently mostly non-microchipped in all the assemblages; the highest frequency of microchipping is in SMR-1W ($N=85$, 42.3%; SI Table 4). Levallois recurrent flakes show the highest frequency of microchipping across all assemblages. Non-facetted platforms are common across blank types and all assemblages. The highest frequency of platform facetting is in Levallois recurrent flakes and core-edge flakes, especially those in SMR-1W (Table 10).

Dimensions

Core dimensions overlap across the most represented categories (Levallois, hierarchical discoid and discoid) and assemblages (Table 11). Despite the differences in medians, no statistical difference has been detected ($p>0.005$), due to the small samples.

The flaking angles overlap widely as well between core types, and no statistical difference has been detected (Table 12).

Regarding the most represented technological categories simple flakes and Kombewa flakes tend to be the shortest blanks across the assemblages, while core-edge flakes are the longest (Table 13). Also, Levallois recurrent flakes are among the longest blank categories. This mirrors

Table 5 Core negatives and scar pattern across the assemblages

Categories	SMR-1		SMR-1E		SMR-1W		Total	
	N	%	*N*	%	*N*	%	*N*	%
Centripetal	12	66.7	4	33.3	7	42.9	23	50.0
Flakes	**12**	**100.0**		**100.0**	**7**	**100.0**	**23**	**100.0**
Centripetal		0.0	1	25.0		0.0	1	4.5
Discoid	1	8.3		0.0		0.0	1	4.5
Expedient		0.0		0.0	1	16.7	1	4.5
Hierarchical Discoid	4	33.3	1	25.0	1	16.7	6	27.3
Levallois	7	58.3	2	50.0	5	66.7	14	59.1
Unidirectional	**5**	**27.8**	**9**	**66.7**	**9**	**57.1**	**23**	**47.7**
Blades		**0.0**	**1**	**0.0**		**0.0**	**1**	**0.0**
Prismatic			1				1	
Bladelets		**0.0**		**0.0**	**1**	**12.5**	**1**	**4.8**
Prismatic					1	100.0	1	100.0
Blades and Flakes		**0.0**	**2**	**25.0**	**1**	**0.0**	**3**	**9.5**
Levallois			1	50.0	1		2	50.0
Levallois and Hierarchical Discoid			1	50.0			1	50.0
Flakes	**5**	**100.0**	**6**	**75.0**	**7**	**87.5**	**18**	**85.7**
Discoid		0.0		0.0	1	14.3	1	5.6
Expedient		0.0	1	16.7	1	14.3	2	11.1
Hierarchical Discoid		0.0	2	33.3	2	28.6	4	22.2
Levallois	3	60.0	3	50.0	3	42.9	9	50.0
SSDA	2	40.0		0.0		0.0	2	11.1
Bidirectional	**1**	**5.6**		**0.0**		**0.0**	**1**	**2.3**
Blades	**1**	**100.0**					**1**	**100.0**
Levallois	1	100.0					1	100.0
Total	**18**	**100.0**	**13**	**100.0**	**16**	**100.0**	**47**	**100.0**

Table 6 Platform preparation in the different core types across all the assemblages

Categories	SMR-1		SMR-1E		SMR-1W		Total	
	N	%	*N*	%	*N*	%	*N*	%
Levallois	**11**	**61.1**	**6**	**50.0**	**9**	**50.0**	**26**	**54.5**
Facetted	9	81.8	5	83.3	7	71.4	21	79.2
Plain		0.0	1	16.7	2	28.6	3	12.5
Natural	2	18.2		0.0		0.0	2	8.3
Hierarchical Discoid	**4**	**22.2**	**3**	**25.0**	**3**	**21.4**	**10**	**22.7**
Plain		0.0	2	66.7	3	100.0	5	50.0
Facetted	3	75.0	1	33.3		0.0	4	40.0
Natural	1	25.0		0.0		0.0	1	10.0
Expedient		**0.0**	**1**	**8.3**	**2**	**14.3**	**3**	**6.8**
Plain			1	100.0	1	50.0	2	66.7
Natural				0.0	1	50.0	1	33.3
SSDA	**2**	**11.1**		**0.0**		**0.0**	**2**	**4.5**
Plain	2	100.0					2	100.0
Discoid	**1**	**5.6**		**0.0**	**1**	**7.1**	**2**	**4.5**
Plain	1	100.0				0.0	1	50.0
Natural		0.0			1	100.0	1	50.0
Levallois and Hierarchical Discoid		**0.0**	**1**	**8.3**		**0.0**	**1**	**2.3**
Facetted			1	100.0			1	100.0
Centripetal		**0.0**	**1**	**8.3**		**0.0**	**1**	**2.3**
Plain			1	100.0			1	100.0
Prismatic		**0.0**	**1**	**0.0**	**1**	**7.1**	**2**	**2.3**
Plain					1	100.0	1	100.0
Natural			1			0.0	1	0.0
Total	**18**	**100.0**	**13**	**100.0**	**16**	**100.0**	**47**	**100.0**

Fig. 7 Cortical and Kombewa flakes. Extensively cortical flakes: SMR-1E PP102 1015, SMR-1W K23 76, SMR-1 P11 729, SMR-1E KK103 933, SMR-1E KK105 904, SMR-1E JJ107 859, SMR-1 M9 267. Kombewa flakes: SMR-1 I13 83, SMR-1W 414 (retouched), SMR-1 K15 2002, SMR-1 O10 601, SMR-1 M12 355, SMR-1W Q25 471. (Photographs by Elisabetta Starnini)

statistical differences between the Levallois recurrent flakes and the core-edge flakes and the simple and Kombewa flakes, regarding length. Differences in width are statistically significant only in SMR-1. Simple flakes and Kombewa flakes are statistically thinner than the rest (Table 13). Core-edge flakes, cortical flakes, and discoid flakes are the thickest blank categories, and they are statistically different from the thinnest blanks categories: simple flakes, Kombewa flakes, and Levallois recurrent flakes (Table 13). Considering only complete, unretouched artefacts with a linear size (maximum length combined with width) larger than 40 mm, Levallois recurrent blanks are confirmed to be the thinnest and flatter knapping products within the assemblages (Table 13).

Levallois recurrent flakes and Kombewa flakes knapping angles differ from those of the discoid flakes as the internal platform angle is narrower and the external platform angle is wider, indicating a more parallel knapping regarding the flaking surface (Table 14).

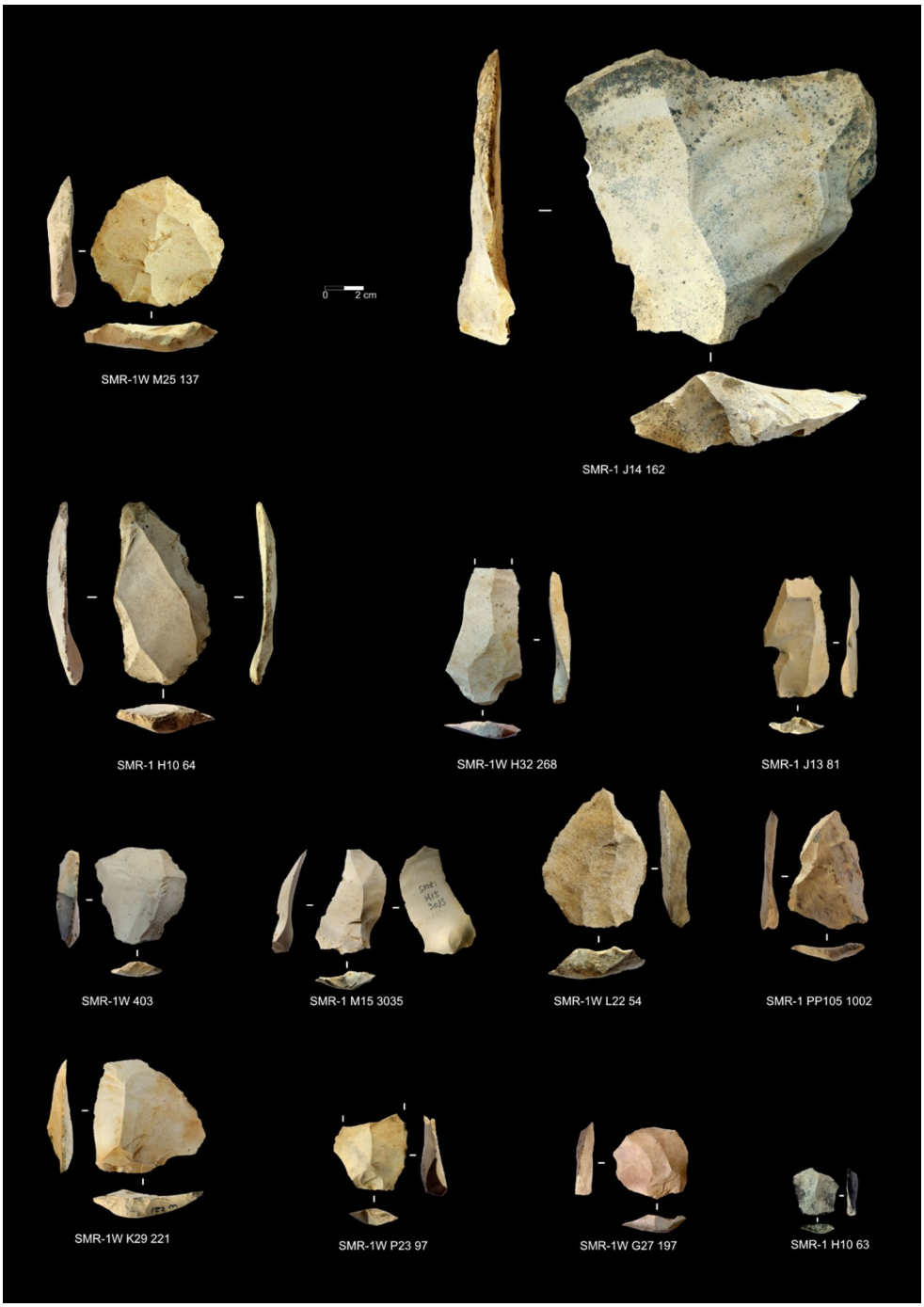

Fig. 8 Levallois flakes. Preferential Levallois flakes: SMR-1W M25 137, SMR-1 J14 162. Levallois blades: SMR-1 H10 64, SMR-1W H32 268, SMR-1 J13 81. Recurrent Levallois flakes: SMR-1W 403, SMR-1 M15 3035, SMR-1W L22 54, SMR-1W K29 221, SMR-1W P23 97, SMR-1W G27 197, SMR-1 H10 63. Levallois point: SMR-1E PP105 1002. (Photographs by Elisabetta Starnini)

Retouched Artefacts

Twenty-eight artefacts exhibit intentional modifications consistent with retouch (Fig. 10). These pieces are manufactured on a diverse range of blank types, including core-convexity management products such as core-edge flakes and overshot flakes. Among them, Levallois recurrent flakes ($N=7$; Table 15) represent the most frequent blank category. The retouched types are predominantly sidescrapers, ranging from simple to bilateral and transversal forms (Table 15; Fig. 11). They also include a Mousterian point. Most of the retouched blanks come from the SMR-1W assemblage.

Raw Material Economy

The assemblage is overwhelmingly fashioned on creamy white, homogeneous, dull, and opaque raw material with a rough, beige cortex (Table 16). This has been petrographically recognised as siliceous limestone (Biagi et al., 2017). Few debitage products are fashioned on other chert types,

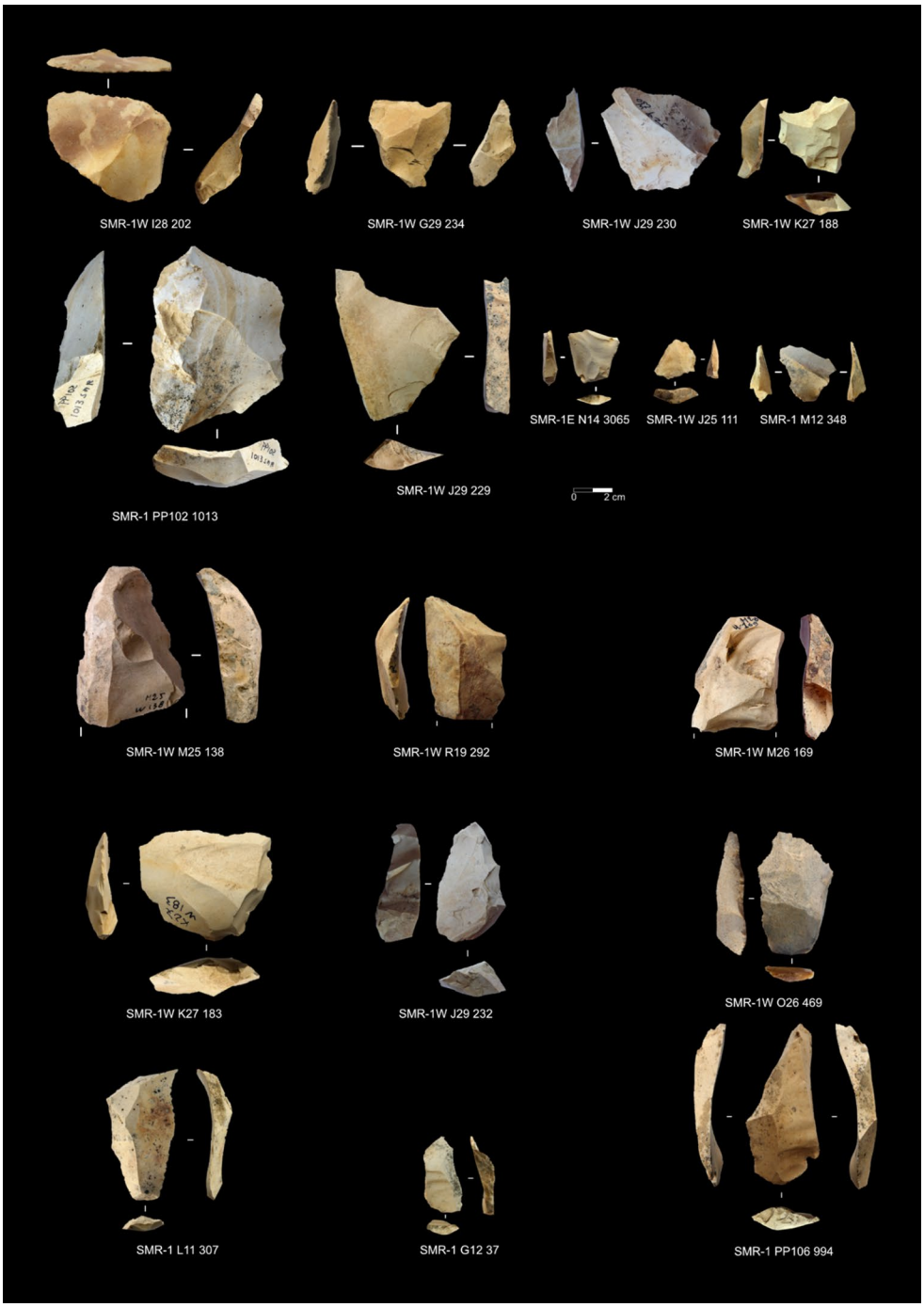

Fig. 9 Core-edge flakes: SMR-1E PP102 1013, SMR-1W J29 229, SMR-1W M25 138, SMR-1W R19 292, SMR-1W M26 169, SMR-1W, K27 183, SMR-1W J29 232, SMR-1W O26 469, SMR-1 L11 307, SMR-1 G12 37, SMR-1E PP106 99. Pseudo-Levallois points: SMR-1W I28 202, SMR-1W G29 234, SMR-1W J29 230, SMR-1W K27 188, SMR-1E N14 3065, SMR-1W J25 111, SMR-1 M12 348. (Photographs by Elisabetta Starnini)

including a grey-green homogeneous, opaque one and a reddish, homogeneous, shiny one (Fig. 11). Most of them are macroscopically identifiable as radiolarite; the other are cherts of unknown petrographic types. The exact sources of procurement are still unknown; nevertheless, radiolarite is available on the Pindos near the village of Avdella (Ozsvárt et al., 2012) and along the slopes of Mt. Vasilitsa, about 14 km from SMR1 as the crow flies. Green chert has been found around Mt. Vasilitsa during surveys.

SMR1: The Lithic Assemblage and the *Chaîne Opératoire* Reconstruction

Three Patches, One Concept

The evidence of SMR1, despite being a surface concentration, shows internal coherence. The technological analysis of the SMR1 industry highlights the presence of

Table 7 Technological types in blanks across the assemblages

Technological type	SMR-1		SMR-1E		SMR-1W		SMR1-exc		Total	
	N	%	*N*	%	*N*	%	*N*	%	*N*	%
Flake	340	42.1	67	31.5	109	28.7	3	75.0	519	37.0
Levallois Recurrent Flake	107	13.2	41	18.8	88	22.1		0.0	236	16.4
Predetermining Flake	105	13.0	18	8.5	47	12.0	1	25.0	171	12.1
Kombewa Flake	93	11.5	25	11.7	22	5.6		0.0	140	9.9
Core-Edge Flake	59	7.3	25	11.3	53	13.6		0.0	137	9.6
Overshot Flake	40	5.0	7	3.3	23	5.9		0.0	70	4.9
Cortical Flake	19	2.4	13	6.1	10	2.4		0.0	42	2.9
Pseudo-Levallois point	11	1.4	3	1.4	9	2.4		0.0	23	1.6
Levallois Blade	11	1.4	4	1.4	11	2.9		0.0	26	1.8
Discoid Centripetal Flake	8	1.0	5	2.3	6	1.6		0.0	19	1.4
Discoid Core-Edge Flake	6	0.7	3	1.4	2	0.3		0.0	11	0.7
Levallois Preferential Flake	4	0.5	1	0.5	8	2.1		0.0	13	0.9
Blade	3	0.4	1	0.5		0.0		0.0	4	0.3
Bladelet	1	0.1	2	0.9	2	0.5		0.0	5	0.4
Crest	1	0.1		0.0		0.0		0.0	1	0.1
Levallois point		0.0	1	0.5		0.0		0.0	1	0.1
Total	**808**	**100.0**	**216**	**100.0**	**390**	**100.0**	**4**	**100.0**	**1418**	**100.0**

a homogeneous lithic assemblage, featuring all stages of reduction and on-site knapping.

From a taphonomic point of view, the three erosional patches show the same degree of edge damage and patina. Nevertheless, the spatial configuration and the content of each patch suggest that SMR-1W might be affected by run-off, with a bias in the preservation of smaller artefacts. This is due to the hill configuration, as the slope is steeper there. Instead, SMR-1, the central erosional patch, is an almost horizontal surface. The evidence from the soil profile at the upper edge of the erosional patch (Fig. 5), and the limited test-pit (Fig. 4) suggest that lithics were embedded in the soil and were left in place by the erosion of the topsoil. Additional proof of preservation is the recovery of two conjoining pieces in two neighbouring squares (Fig. 4).

Nevertheless, even though the three assemblages are not identical, they are not significantly different. Hence it is safe to treat them as part of the same chronological and behavioural occupations.

Raw material procurement is heavily focused on siliceous limestone that is available all along the Delichmét - Mt. Kirkouri ridge and slopes, right in front of site SMR1 (Fig. 12; Biagi et al., 2015, 2017). Within a limestone formation there are round nodules of raw material with conchoid fracture readily available on the surface (Fig. 12). The petrographic analysis of geological samples noticed the composite nature of the material, consisting of layers of limestone, siliceous limestone, calcareous chert, non-calcareous chert, and chalcedony (Biagi et al., 2017).

The round nodules can be split open, removing flakes with a spherical cap shape, ca. 100×150 mm large on average, though they can reach up to 600 mm in length (Figs. 12 and 13). The SMR1 cores and the presence of decortication workshops on the Delichmét - Mt. Kirkouri ridge (Biagi et al., 2015, 2017) support the hypothesis that this was the primary mode of raw material import to the site. Once the spherical cap is obtained, it can be easily turned so that the cortical surface is transformed into the striking platform, and the former ventral surface is turned into the flaking surface (Fig. 14). After the first spherical cap is removed, several others can be detached using the negative of the first one to remove the others on the nodule side. These secondary spherical caps have a non-cortical 90° surface that can be turned preferentially on a striking platform.

This raw material procurement mode explains the small percentage of fully or extensively cortical artefacts, as the original flaking surface is a ventral one. Essentially, the first flakes will be Kombewa, removing the ventral face of the spherical cap. The rest of the reduction follows a classical Levallois recurrent reduction. There is no evidence of bifacial reduction, as it would be expected in a classical discoid method; in one case, the core has effectively two exploited flaking surfaces on the upper and lower surfaces. Nevertheless, these reductions are independent and carried out on a single surface at a time. Technologically and typologically, the SMR1 assemblage can be attributed to the Middle Palaeolithic mode of production. In fact, there are no predominant traces of volumetric blade and bladelet cores. In particular, there is one bladelet prismatic core, which may combine with the few bladelets found in the assemblage. A volumetric bladelet production is found associated with more typical Middle Palaeolithic reduction in secure Middle Palaeolithic contexts (Carmignani & Soressi, 2023).

Table 8 Cortex percentage and location in blanks across the assemblages

Categories	SMR-1		SMR-1E		SMR-1W		SMR1-exc		Total	
	N	%	*N*	%	*N*	%	*N*	%	*N*	%
No Cortex	**718**	**88.9**	**182**	**84.5**	**319**	**81.6**	**3**	**75.0**	**1222**	**86.2**
Blade	3	0.4	1	0.6		0.0		0.0	4	0.3
Bladelet	1	0.1	2	1.1	2	0.7		0.0	5	0.4
Core-Edge Flake	39	5.4	13	7.2	27	8.1		0.0	79	6.4
Crest	1	0.1		0.0		0.0		0.0	1	0.1
Discoid Centripetal Flake	6	0.8	5	2.8	4	1.3		0.0	15	1.2
Discoid Core-Edge Flake	4	0.6	2	1.1	2	0.3		0.0	8	0.6
Flake	326	45.4	65	36.1	107	34.5	3	100.0	501	41.4
Kombewa Flake	92	12.8	24	13.3	22	6.8		0.0	138	11.3
Levallois Blade	10	1.4	4	1.7	9	2.9		0.0	23	1.8
Levallois point		0.0	1	0.6		0.0		0.0	1	0.1
Levallois Preferential Flake	3	0.4	1	0.6	6	2.0		0.0	10	0.8
Levallois Recurrent Flake	105	14.6	38	20.6	83	25.4		0.0	226	18.2
Overshot Flake	21	2.9	5	2.8	13	4.2		0.0	39	3.2
Predetermining Flake	97	13.5	18	10.0	37	11.4		0.0	152	12.4
Pseudo-Levallois point	10	1.4	3	1.7	7	2.3		0.0	20	1.7
Presence of Cortex	**90**	**11.1**	**34**	**15.5**	**71**	**18.4**	**1**	**25.0**	**196**	**13.8**
<50	**65**	**72.2**	**20**	**57.6**	**52**	**73.9**	**1**	**100.0**	**138**	**70.5**
Distal	*24*	*36.9*	*5*	*26.3*	*15*	*27.5*		*0.0*	*44*	*31.6*
Core-Edge Flake		0.0	3	60.0	2	14.3			5	11.6
Discoid Centripetal Flake	2	8.3		0.0	2	14.3			4	9.3
Discoid Core-Edge Flake	1	4.2		0.0		0.0			1	2.3
Flake	2	8.3		0.0	1	7.1			3	7.0
Levallois Recurrent Flake	1	4.2		0.0	4	28.6			5	11.6
Overshot Flake	13	54.2	2	40.0	5	28.6			20	44.2
Predetermining Flake	5	20.8		0.0	1	7.1			6	14.0
Distal & Lateral		*0.0*		*0.0*	*1*	*2.0*		*0.0*	*1*	*0.7*
Core-Edge Flake					1	100.0			1	100.0
Dorsal	*6*	*9.2*		*0.0*	*3*	*5.9*		*0.0*	*9*	*6.6*
Cortical Flake	2	33.3				0.0			2	22.2
Levallois Blade	1	16.7				0.0			1	11.1
Levallois Preferential Flake	1	16.7				0.0			1	11.1
Predetermining Flake	1	16.7			3	100.0			4	44.4
Pseudo-Levallois point	1	16.7				0.0			1	11.1
Lateral	*26*	*40.0*	*12*	*57.9*	*27*	*52.9*	*1*	*100.0*	*66*	*47.8*
Core-Edge Flake	15	57.7	8	63.6	17	63.0		0.0	40	60.0
Cortical Flake	1	3.8	1	9.1		0.0		0.0	2	3.1
Discoid Core-Edge Flake		0.0	1	9.1		0.0		0.0	1	1.5
Flake	8	30.8	1	9.1		0.0		0.0	9	13.8
Kombewa Flake		0.0	1	9.1		0.0		0.0	1	1.5
Levallois Preferential Flake		0.0		0.0	1	3.7		0.0	1	1.5
Levallois Recurrent Flake		0.0		0.0	1	3.7		0.0	1	1.5
Overshot Flake	2	7.7		0.0	4	14.8		0.0	6	9.2
Predetermining Flake		0.0		0.0	2	7.4	1	100.0	3	4.6
Pseudo-Levallois point		0.0		0.0	2	7.4		0.0	2	3.1
Lateral & Distal	*2*	*3.1*		*0.0*		*0.0*		*0.0*	*2*	*1.5*
Core-Edge Flake	1	50.0							1	50.0
Overshot Flake	1	50.0							1	50.0
NA		*0.0*		*0.0*	*1*	*2.0*		*0.0*	*1*	*0.7*
Flake					1	100.0			1	100.0
Proximal	*7*	*10.8*	*3*	*15.8*	*5*	*9.8*		*0.0*	*15*	*11.0*
Core-Edge Flake	2	28.6	1	33.3	1	20.0			4	26.7
Discoid Core-Edge Flake	1	14.3		0.0		0.0			1	6.7
Flake	1	14.3	1	33.3		0.0			2	13.3

Table 8 (continued)

Categories	SMR-1		SMR-1E		SMR-1W		SMR1-exc		Total	
	N	%	*N*	%	*N*	%	*N*	%	*N*	%
Kombewa Flake	1	14.3		0.0		0.0			1	6.7
Levallois Blade		0.0		0.0	1	20.0			1	6.7
Levallois Preferential Flake		0.0		0.0	1	20.0			1	6.7
Levallois Recurrent Flake	1	14.3	1	33.3		0.0			2	13.3
Predetermining Flake	1	14.3		0.0	2	40.0			3	20.0
50	**7**	**7.8**	**4**	**12.1**	**12**	**15.9**		**0.0**	**23**	**11.4**
Distal	*2*	*28.6*	*1*	*25.0*	*2*	*18.2*			*5*	*22.7*
Cortical Flake		0.0	1	100.0	2	100.0			3	60.0
Overshot Flake	1	50.0		0.0		0.0			1	20.0
Predetermining Flake	1	50.0		0.0		0.0			1	20.0
Dorsal	*4*	*57.1*		*0.0*		*0.0*			*4*	*18.2*
Core-Edge Flake	1	25.0							1	25.0
Cortical Flake	2	50.0							2	50.0
Flake	1	25.0							1	25.0
Lateral	*1*	*14.3*	*3*	*75.0*	*10*	*81.8*			*14*	*59.1*
Core-Edge Flake		0.0		0.0	3	33.3			3	23.1
Cortical Flake		0.0	2	66.7	3	22.2			5	30.8
Flake	1	100.0		0.0		0.0			1	7.7
Levallois Blade		0.0		0.0	1	11.1			1	7.7
Levallois Recurrent Flake		0.0	1	33.3		0.0			1	7.7
Overshot Flake		0.0		0.0	1	11.1			1	7.7
Predetermining Flake		0.0		0.0	2	22.2			2	15.4
>50	**11**	**12.2**	**5**	**15.2**	**2**	**2.9**		**0.0**	**18**	**9.3**
Dorsal	*9*	*81.8*	*5*	*100.0*	*2*	*100.0*			*16*	*88.9*
Core-Edge Flake	1	11.1		0.0	1	50.0			2	12.5
Cortical Flake	6	66.7	4	80.0	1	50.0			11	68.8
Flake	1	11.1		0.0		0.0			1	6.3
Levallois Recurrent Flake		0.0	1	20.0		0.0			1	6.3
Overshot Flake	1	11.1		0.0		0.0			1	6.3
Lateral & Distal	*1*	*9.1*		*0.0*		*0.0*	*1*			*5.6*
Overshot Flake	1	100.0							1	100.0
Proximal	*1*	*9.1*	*0.0*			*0.0*	*1*			*5.6*
Cortical Flake	1	100.0							1	100.0
100	**7**	**7.8**	**5**	**15.2**	**5**	**7.2**		**0.0**	**17**	**8.8**
Dorsal	*7*	*100.0*	*5*	*100.0*	*4*	*80.0*			*16*	*94.1*
Cortical Flake	7	100.0	5	100.0	4	100.0			16	100.0
Dorsal & Lateral		*0.0*		*0.0*	*1*	*20.0*			*1*	*5.9*
Core-Edge Flake					1	100.0			1	100.0
Total	**808**	**100.0**	**216**	**100.0**	**390**	**100.0**	**4**	**100.0**	**1418**	**100.0**

Discoid vs. Levallois

Discerning between discoid, especially unifacial hierarchical discoid knapping, and centripetal Levallois is complex (Boëda, 1993; Bustos-Pérez et al., 2023; Delpiano et al., 2021; González-Molina et al., 2020; Peresani, 2003). In SMR1 there are only two cores that can be defined as bifacial discoid; the rest of the discoidal cores are defined as hierarchical discoid, as they use a single flaking surface. Nevertheless, the flaking angle in cores is not statistically different from Levallois recurrent cores. The debitage products are largely consistent with a surface exploitation, i.e. Levallois *sensu latu*. At SMR1 there is a consistent production of large and thin flakes, which exploits predetermined convexities. The convexities management is embedded in the reduction, partially removing core-edge products (core-edge flakes, pseudo-Levallois points, overshot flakes). Comparing statistically SMR1 blanks with those from controlled experimental knapping published by Bustos-Peréz and colleagues (2023), SMR1 Levallois recurrent flakes internal and external platform angles are different from those of the discoid and

Table 9 Blank negatives and scar patterns across the assemblages subdivided by scar patterns, with relative frequencies of negative types within the scar patterns and technological types

Categories	SMR-1		SMR-1E		SMR-1W		SMR1-exc		Total	
	N	%	N	%	N	%	N	%	N	%
Unidirectional	**405**	**56.3**	**98**	**50.3**	**193**	**53.1**	**1**	**25.0**	**697**	**54.4**
Flakes	**353**	**87.2**	**76**	**79.2**	**149**	**76.6**		**0.0**	**578**	**83.0**
Bladelet	1	0.3	1	1.3		0.0			2	0.3
Core–Edge Flake	15	4.2	3	3.9	15	10.4			33	5.8
Cortical Flake	7	2.0	6	7.9	1	0.7			14	2.4
Discoid Centripetal Flake	4	1.1	1	1.3	1	0.7			6	1.0
Discoid Core–Edge Flake	1	0.3		0.0		0.0			1	0.2
Flake	164	46.5	31	40.8	51	35.4			246	42.9
Kombewa Flake	28	7.9	7	9.2	7	4.9			42	7.3
Levallois Blade	1	0.3	1	1.3	2	1.4			4	0.7
Levallois Preferential Flake	2	0.6		0.0		0.0			2	0.3
Levallois Recurrent Flake	49	13.9	14	18.4	38	24.3			101	17.1
Overshot Flake	21	5.9	3	3.9	14	9.0			38	6.5
Predetermining Flake	55	15.6	8	10.5	18	11.8			81	14.0
Pseudo-Levallois point	5	1.4	1	1.3	2	1.4			8	1.4
Flakes and Blades	**1**	**0.2**		**0.0**	**1**	**0.5**		**0.0**	**2**	**0.3**
Levallois Blade	1	100.0				0.0			1	50.0
Levallois Recurrent Flake		0.0			1	100.0			1	50.0
Bladelets	**1**	**0.2**		**0.0**		**0.0**		**0.0**	**1**	**0.1**
Predetermining Flake	1	100.0							1	100.0
Blades	**2**	**0.5**	**3**	**2.1**		**0.0**		**0.0**	**5**	**0.6**
Core–Edge Flake	1	50.0		0.0					1	25.0
Levallois Blade		0.0	2	50.0					2	25.0
Overshot Flake	1	50.0	1	50.0					2	50.0
Not determined negatives' type	**48**	**11.9**	**19**	**18.8**	**43**	**22.9**	**1**	**100.0**	**111**	**15.9**
Blade	2	4.2		0.0		0.0		0.0	2	1.8
Bladelet		0.0	1	5.6	2	4.7		0.0	3	2.7
Core–Edge Flake	9	18.8	9	44.4	11	25.6		0.0	29	25.5
Cortical Flake		0.0		0.0	1	2.3		0.0	1	0.9
Flake	8	16.7	1	5.6	9	20.9	1	100.0	19	17.3
Kombewa Flake		0.0		0.0	2	4.7		0.0	2	1.8
Levallois Blade	4	8.3	1	5.6	7	16.3		0.0	12	10.9
Levallois Recurrent Flake	15	31.3	7	38.9	6	14.0		0.0	28	25.5
Overshot Flake	8	16.7		0.0	2	4.7		0.0	10	9.1
Predetermining Flake	2	4.2		0.0	3	7.0		0.0	5	4.5
Centripetal	**155**	**21.6**	**51**	**26.7**	**102**	**26.8**	**1**	**25.0**	**309**	**23.8**
Flakes	**151**	**97.4**	**50**	**98.0**	**100**	**97.9**	**1**	**100.0**	**302**	**97.7**
Core–Edge Flake	14	9.3	4	8.0	10	9.7		0.0	28	9.2
Cortical Flake	1	0.7	1	2.0	3	2.2		0.0	5	1.4
Crest	1	0.7		0.0		0.0		0.0	1	0.3
Discoid Centripetal Flake	3	2.0	3	6.0	4	4.3		0.0	10	3.4
Discoid Core–Edge Flake	1	0.7	3	6.0	1	0.0		0.0	5	1.4
Flake	61	40.4	16	32.0	23	23.7	1	100.0	101	33.9
Kombewa Flake	4	2.6		0.0	1	1.1		0.0	5	1.7
Levallois Blade	1	0.7		0.0		0.0		0.0	1	0.3
Levallois Preferential Flake	2	1.3	1	2.0	5	5.4		0.0	8	2.7
Levallois Recurrent Flake	33	21.9	14	28.0	29	29.0		0.0	76	25.1
Overshot Flake	4	2.6	2	4.0	5	5.4		0.0	11	3.7
Predetermining Flake	23	15.2	5	10.0	13	12.9		0.0	41	13.6
Pseudo-Levallois point	3	2.0	1	2.0	6	6.5		0.0	10	3.4
Not determined negative's type	**4**	**2.6**	**1**	**2.0**	**2**	**2.1**		**0.0**	**7**	**2.3**
Blade	1	25.0		0.0		0.0			1	14.3
Core–Edge Flake	1	25.0	1	100.0		0.0			2	28.6

Table 9 (continued)

Categories	SMR-1		SMR-1E		SMR-1W		SMR1-exc		Total	
	N	%	N	%	N	%	N	%	N	%
Discoid Centripetal Flake	1	25.0		0.0		0.0			1	14.3
Levallois Recurrent Flake		0.0		0.0	1	50.0			1	14.3
Predetermining Flake	1	25.0		0.0	1	50.0			2	28.6
Unidirectional-Crossed	**78**	**10.8**	**33**	**16.8**	**36**	**10.2**		**0.0**	**147**	**11.5**
Flakes	**73**	**93.6**	**28**	**87.5**	**33**	**91.7**			**134**	**91.8**
Core–Edge Flake	12	16.4	3	10.7	9	27.3			24	17.9
Cortical Flake	2	2.7	1	3.6	1	3.0			4	3.0
Flake	30	41.1	8	28.6	6	18.2			44	32.8
Kombewa Flake	6	8.2	7	25.0	3	9.1			16	11.9
Levallois Recurrent Flake	5	6.8	4	14.3	6	18.2			15	11.2
Overshot Flake	1	1.4	1	3.6	1	3.0			3	2.2
Predetermining Flake	14	19.2	4	14.3	7	21.2			25	18.7
Pseudo-Levallois point	3	4.1		0.0		0.0			3	2.2
Blades	**1**	**1.3**		**0.0**		**0.0**			**1**	**0.7**
Levallois Recurrent Flake	1	100.0							1	100.0
Not determined negatives' type	**4**	**5.1**	**5**	**12.5**	**3**	**8.3**			**12**	**7.5**
Core–Edge Flake		0.0	1	25.0		0.0			1	9.1
Cortical Flake	1	25.0		0.0		0.0			1	9.1
Flake	1	25.0	1	25.0		0.0			2	18.2
Levallois Blade	1	25.0		0.0		0.0			1	9.1
Levallois Recurrent Flake	1	25.0	2	25.0		0.0			3	18.2
Predetermining Flake		0.0		0.0	3	100.0			3	27.3
Pseudo-Levallois point		0.0	1	25.0		0.0			1	9.1
Not determined negative direction	**55**	**7.6**	**4**	**2.1**	**11**	**3.1**	**1**	**25.0**	**71**	**5.6**
Flakes	**52**	**94.5**	**4**	**100.0**	**8**	**72.7**		**0.0**	**64**	**90.1**
Core–Edge Flake		0.0		0.0	1	12.5			1	1.6
Flake	45	86.5	4	100.0	7	87.5			56	87.5
Kombewa Flake	6	11.5		0.0		0.0			6	9.4
Predetermining Flake	1	1.9		0.0		0.0			1	1.6
Not determined negatives' type	**3**	**5.5**		**0.0**	**3**	**27.3**	**1**	**100.0**	**7**	**9.9**
Flake	2	66.7			2	66.7	1	100.0	5	71.4
Kombewa Flake	1	33.3			1	33.3		0.0	2	28.6
Unidirectional & Crossed	**7**	**1.0**	**4**	**2.1**	**9**	**2.5**	**1**	**25.0**	**21**	**1.7**
Flakes	**5**	**71.4**	**3**	**75.0**	**7**	**77.8**	**1**	**100.0**	**16**	**76.2**
Core–Edge Flake	1	20.0	1	33.3	1	14.3		0.0	3	18.8
Discoid Centripetal Flake		0.0	1	33.3		0.0		0.0	1	6.3
Levallois Blade	1	20.0		0.0	1	14.3		0.0	2	12.5
Levallois Recurrent Flake		0.0		0.0	3	42.9		0.0	3	18.8
Overshot Flake		0.0		0.0	1	14.3		0.0	1	6.3
Predetermining Flake	3	60.0	1	33.3	1	14.3	1	100.0	6	37.5
Not determined negatives' type	**2**	**28.6**	**1**	**25.0**	**2**	**22.2**		**0.0**	**5**	**23.8**
Core–Edge Flake		0.0	1	100.0		0.0			1	20.0
Levallois Blade	1	50.0		0.0		0.0			1	20.0
Levallois Recurrent Flake		0.0		0.0	2	100.0			2	40.0
Predetermining Flake	1	50.0		0.0		0.0			1	20.0
Bidirectional	**13**	**1.8**	**2**	**1.0**	**7**	**1.7**		**0.0**	**22**	**1.7**
Flakes	**8**	**61.5**	**1**	**50.0**	**4**	**66.7**			**13**	**61.9**
Core–Edge Flake	1	12.5		0.0		0.0			1	7.7
Flake	1	12.5	1	100.0	2	50.0			4	30.8
Kombewa Flake		0.0		0.0	1	25.0			1	7.7
Levallois Recurrent Flake	1	12.5		0.0	1	25.0			2	15.4
Overshot Flake	3	37.5		0.0		0.0			3	23.1
Predetermining Flake	2	25.0		0.0		0.0			2	15.4

Table 9 (continued)

Categories	SMR-1		SMR-1E		SMR-1W		SMR1-exc		Total	
	N	%	N	%	N	%	N	%	N	%
Blades	**2**	**15.4**		**0.0**		**0.0**			**2**	**9.5**
Levallois Blade	1	50.0							1	50.0
Overshot Flake	1	50.0							1	50.0
Not determined negatives' type	**3**	**23.1**	**1**	**50.0**	**3**	**33.3**			**7**	**28.6**
Blade		0.0	1	100.0		0.0			1	16.7
Core–Edge Flake	2	66.7		0.0	1	0.0			3	33.3
Flake		0.0		0.0	1	50.0			1	16.7
Levallois Blade		0.0		0.0	1	50.0			1	16.7
Levallois Recurrent Flake	1	33.3		0.0		0.0			1	16.7
Unidirectional & Secant	**3**	**0.4**		**0.0**	**3**	**0.8**		**0.0**	**6**	**0.5**
Flakes	**3**	**100.0**			**3**	**100.0**			**6**	**100.0**
Core–Edge Flake		0.0			2	66.7			2	33.3
Discoid Core–Edge Flake	2	66.7			1	33.3			3	50.0
Overshot Flake	1	33.3				0.0			1	16.7
Crossed & Secant	**1**	**0.1**		**0.0**	**2**	**0.6**		**0.0**	**3**	**0.2**
Flakes	**1**	**100.0**			**2**	**100.0**			**3**	**100.0**
Discoid Centripetal Flake		0.0			1	50.0			1	33.3
Discoid Core–Edge Flake	1	100.0				0.0			1	33.3
Pseudo-Levallois point		0.0			1	50.0			1	33.3
Unidirectional-Convergent	**1**	**0.1**	**1**	**0.5**		**0.0**		**0.0**	**2**	**0.2**
Flakes	**1**	**100.0**	**1**	**100.0**					**2**	**100.0**
Levallois point		0.0	1	100.0					1	50.0
Levallois Recurrent Flake	1	100.0		0.0					1	50.0
Unidirectional & Centripetal		**0.0**		**0.0**	**2**	**0.6**		**0.0**	**2**	**0.2**
Flakes					**1**	**50.0**			**1**	**50.0**
Levallois Preferential Flake					1	100.0			1	100.0
Flakes and Blades					**1**	**50.0**			**1**	**50.0**
Levallois Preferential Flake					1	100.0			1	100.0
Secant		**0.0**	**1**	**0.5**		**0.0**		**0.0**	**1**	**0.1**
Flakes			**1**	**100.0**					**1**	**100.0**
Core–Edge Flake			1	100.0					1	100.0
Crossed & Centripetal		**0.0**		**0.0**	**1**	**0.3**		**0.0**	**1**	**0.1**
Flakes					**1**	**100.0**			**1**	**100.0**
Levallois Recurrent Flake					1	100.0			1	100.0
Crossed & Unidirectional		**0.0**		**0.0**	**1**	**0.3**		**0.0**	**1**	**0.1**
Flakes					**1**	**100.0**			**1**	**100.0**
Levallois Preferential Flake					1	100.0			1	100.0
Centripetal & Secant	**1**	**0.1**		**0.0**		**0.0**		**0.0**	**1**	**0.1**
Flakes	**1**	**100.0**							**1**	**100.0**
Discoid Core–Edge Flake	1	100.0							1	100.0
Total	**719**	**100.0**	**194**	**100.0**	**367**	**100.0**	**4**	**100.0**	**1284**	**100.0**

hierarchical discoid experimental reductions (Table 17). SMR1 core-edge flakes internal and external platform angles are statistically different from those of hierarchical discoid backed flakes from the experimental knapping (Table 17). Hence, it can be deduced that SMR1 blanks have angles mostly comparable with Levallois experimental reductions and different from a bifacial, and more importantly, unifacial discoid reduction. Moreover, all evidence points to assigning SMR1 knapping products to a Levallois-type reduction.

Unidirectional, Centripetal Knapping or both?

While cores in general show an equal split between centripetal and unidirectional scar patterns, blanks mostly display a unidirectional scar pattern. Therefore, the coexistence of unidirectional and centripetal reductions, or the presence of a single reduction sequence switching from unidirectional to centripetal, should be addressed. The coexistence of unidirectional and centripetal reduction patterns is consistent with this production strategy. Assessments based on raw

Table 10 Platform preparation in all the assemblages grouped by technological types

Categories	SMR-1		SMR-1E		SMR-1W		SMR1-exc		Total	
	N	%	*N*	%	*N*	%	*N*	%	*N*	%
Levallois Recurrent Flake	**42**	**22.7**	**15**	**21.1**	**58**	**29.4**		**0.0**	**115**	**25.2**
Non-Facetted	34	81.0	13	86.7	37	63.2			84	72.8
Facetted	6	14.3	2	13.3	11	19.3			19	16.7
Dihedral	1	2.4		0.0	9	15.8			10	8.8
Natural	1	2.4		0.0	1	1.8			2	1.8
Core-Edge Flake	**36**	**19.5**	**18**	**23.9**	**38**	**18.6**		**0.0**	**92**	**19.7**
Non-Facetted	28	77.8	14	76.5	24	61.1			66	70.8
Facetted	4	11.1	3	17.6	7	19.4			14	15.7
Dihedral	3	8.3	1	5.9	3	8.3			7	7.9
Natural	1	2.8		0.0	4	11.1			5	5.6
Predetermining Flake	**20**	**10.8**	**10**	**14.1**	**27**	**13.9**	**1**	**50.0**	**58**	**12.8**
Non-Facetted	17	85.0	8	80.0	21	77.8	1	100.0	47	81.0
Dihedral	1	5.0	1	10.0	4	14.8		0.0	6	10.3
Natural	1	5.0		0.0	2	7.4		0.0	3	5.2
Facetted	1	5.0	1	10.0		0.0		0.0	2	3.4
Overshot Flake	**24**	**13.0**	**5**	**7.0**	**15**	**7.2**		**0.0**	**44**	**9.5**
Non-Facetted	17	70.8	3	60.0	14	92.9			34	76.7
Dihedral	6	25.0	1	20.0	1	7.1			8	18.6
Facetted	1	4.2	1	20.0		0.0			2	4.7
Flake	**19**	**10.3**	**4**	**5.6**	**17**	**8.8**	**1**	**50.0**	**41**	**9.1**
Non-Facetted	15	78.9	3	75.0	12	70.6	1	100.0	31	75.6
Dihedral	2	10.5		0.0	2	11.8		0.0	4	9.8
Facetted	1	5.3	1	25.0	2	11.8		0.0	4	9.8
Natural	1	5.3		0.0	1	5.9		0.0	2	4.9
Cortical Flake	**9**	**4.9**	**6**	**8.5**	**8**	**3.6**		**0.0**	**23**	**4.9**
Non-Facetted	8	88.9	5	83.3	6	71.4			19	81.8
Facetted	1	11.1	1	16.7		0.0			2	9.1
ND		0.0		0.0	2	28.6			2	9.1
Levallois Blade	**9**	**4.9**	**3**	**2.8**	**9**	**4.6**		**0.0**	**21**	**4.4**
Facetted	4	44.4	1	50.0	3	33.3			8	40.0
Non-Facetted	4	44.4	1	0.0	3	33.3			8	35.0
Dihedral	1	11.1		0.0	2	22.2			3	15.0
Natural		0.0	1	50.0	1	11.1			2	10.0
Kombewa Flake	**5**	**2.7**	**2**	**2.8**	**7**	**3.6**		**0.0**	**14**	**3.1**
Non-Facetted	3	60.0	1	50.0	5	71.4			9	64.3
Natural	2	40.0		0.0	1	14.3			3	21.4
Facetted		0.0	1	50.0	1	14.3			2	14.3
Pseudo-Levallois point	**4**	**2.2**	**1**	**1.4**	**7**	**3.6**		**0.0**	**12**	**2.7**
Non-Facetted	4	100.0	1	100.0	5	71.4			10	83.3
Dihedral		0.0		0.0	2	28.6			2	16.7
Discoid Centripetal Flake	**5**	**2.7**	**3**	**4.2**	**4**	**2.1**		**0.0**	**12**	**2.7**
Non-Facetted	5	100.0	2	66.7	3	75.0			10	83.3
Dihedral		0.0	1	33.3		0.0			1	8.3
Facetted		0.0		0.0	1	25.0			1	8.3
Levallois Preferential Flake	**4**	**2.2**	**1**	**1.4**	**6**	**3.1**		**0.0**	**11**	**2.4**
Non-Facetted	2	50.0	1	100.0	3	50.0			6	54.5
Facetted	1	25.0		0.0	2	33.3			3	27.3
Dihedral	1	25.0		0.0		0.0			1	9.1
Natural		0.0		0.0	1	16.7			1	9.1
Discoid Core-Edge Flake	**6**	**3.2**	**3**	**4.2**	**2**	**0.5**		**0.0**	**11**	**2.2**
Non-Facetted	3	50.0	3	100.0	1	0.0			7	60.0
Dihedral	3	50.0		0.0	1	100.0			4	40.0
Blade	**2**	**1.1**	**1**	**1.4**		**0.0**		**0.0**	**3**	**0.7**
Non-Facetted	1	50.0	1	100.0					2	66.7

Table 10 (continued)

Categories	SMR-1		SMR-1E		SMR-1W		SMR1-exc		Total	
	N	%	*N*	%	*N*	%	*N*	%	*N*	%
Facetted	1	50.0		0.0					1	33.3
Bladelet		**0.0**		**0.0**	**2**	**1.0**		**0.0**	**2**	**0.4**
Non-Facetted					2	100.0			2	100.0
Levallois point		**0.0**	**1**	**1.4**		**0.0**		**0.0**	**1**	**0.2**
Facetted			1	100.0					1	100.0
Total	**185**	**100.0**	**73**	**100.0**	**200**	**100.0**	**2**	**100.0**	**460**	**100.0**

Table 11 Minimum, median, maximum dimensions (mm) of complete Discoid, Hierarchical Discoid, and Levallois cores across assemblages

Categories	Assemblage	*N*	Min.	Median	Max.
Length					
Discoid	SMR-1	1	56.5	56.5	56.5
Hierarchical Discoid	SMR-1	3	48.2	67.8	117
Hierarchical Discoid	SMR-1E	3	52.2	53.7	67.0
Hierarchical Discoid	SMR-1W	1	45.5	45.5	45.5
Levallois	SMR-1	6	39.6	53.4	134
Levallois	SMR-1E	6	42.6	54.6	69.6
Levallois	SMR-1W	6	41.8	50.2	72.4
Width					
Discoid	SMR-1	1	41.4	41.4	41.4
Hierarchical Discoid	SMR-1	3	51.9	55.2	96.0
Hierarchical Discoid	SMR-1E	3	40.6	52.2	62.4
Hierarchical Discoid	SMR-1W	1	41.1	41.1	41.1
Levallois	SMR-1	6	33.8	55.3	106
Levallois	SMR-1E	6	34.4	47.2	77.1
Levallois	SMR-1W	6	31.3	56.7	68.4
Thickness					
Discoid	SMR-1	1	27.5	27.5	27.5
Hierarchical Discoid	SMR-1	3	19.2	19.5	40.8
Hierarchical Discoid	SMR-1E	3	14.88	20.6	24.89
Hierarchical Discoid	SMR-1W	1	13.2	13.2	13.2
Levallois	SMR-1	6	14.5	18.4	49.4
Levallois	SMR-1E	6	11.3	17.9	22.5
Levallois	SMR-1W	6	12.8	14.9	26.5

Table 12 Minimum, median, maximum flaking angles (degrees) of complete discoid, hierarchical discoid, and Levallois cores across assemblages

Type	Assemblage	*N*	Min.	median	Max.
Discoid	SMR-1	1	55	55	55
Hierarchical Discoid	SMR-1	3	60	65	70
Hierarchical Discoid	SMR-1E	3	60	70	80
Hierarchical Discoid	SMR-1W	1	80	80	80
Levallois	SMR-1	6	55	65	80
Levallois	SMR-1E	6	40	62.5	70
Levallois	SMR-1W	6	60	65	80

material procurement suggest that centripetal flaking could have been the preferred initial modality for fully cortical spherical caps; in contrast, unidirectional products could be removed more easily from secondary spherical caps using a non-cortical striking platform. There is also evidence of artefacts exhibiting both unidirectional and crossed reduction patterns. In another context where Levallois reduction is predominant, this pattern was interpreted as a laterally migrating striking platform minimizing costly repreparations of the striking platform (Peresani, 2012). This explanation may account for the abundance of unidirectional scar patterns in blanks, reflecting multiple unidirectional extractions. Scatterplots of length versus width for cores and Levallois recurrent flakes reveal a clear positive correlation within each group, indicating consistent shape scaling across the assemblage. Spearman's rank correlations are strong for all groups ($\rho = 0.67–0.88$, $p < 0.01$), confirming that longer flakes tend to be wider regardless of scar direction or type. Examination of the scatter distribution shows that unidirectional Levallois recurrent flakes are generally longer and exhibit greater variation along the length axis, whereas centripetal flakes cluster at shorter lengths, indicating a smaller overall size (Fig. 15). This pattern suggests that centripetal and unidirectional flakes coexisted within the same reduction system, following a common technological logic, with size differences likely reflecting different stages of reduction or core exploitation rather than entirely separate production strategies.

Discussion

The absence of any organic material associated with the lithic assemblage from SMR1 makes it impossible to obtain an absolute date. Nevertheless, its techno-typological characters and the presence of complete reduction sequences allow for comparison with the most important Middle Palaeolithic assemblages so far investigated in the southern Balkans.

The Dated Assemblages in northwestern Greece and Neighbouring Areas

Asprochaliko

Asprochaliko is one of the reference stratigraphies in the Balkan Peninsula, especially concerning the Middle

Table 13 Minimum, median, maximum dimensions (mm) of complete blank categories across assemblages. Mean thickness measured only for blanks with linear size (length combined with width) larger than 39.99 mm

Type	Assemblage	*N*	Min.	Median	Max.
Length					
Core-Edge Flake	SMR-1	44	13.0	41.8	74.6
Core-Edge Flake	SMR-1E	18	24.0	49.9	84.1
Core-Edge Flake	SMR-1W	31	22.3	46.8	114.8
Cortical Flake	SMR-1	11	18.4	28.9	63.1
Cortical Flake	SMR-1E	8	17.6	29.6	89.4
Cortical Flake	SMR-1W	8	24.0	49.6	86.6
Discoid Centripetal Flake	SMR-1	5	28.1	36.4	52.6
Discoid Centripetal Flake	SMR-1E	4	17.0	26.8	45.9
Discoid Centripetal Flake	SMR-1W	4	21.9	28.7	38.1
Discoid Core-Edge Flake	SMR-1	6	17.1	36.6	38.9
Discoid Core-Edge Flake	SMR-1E	3	23.9	40.5	56.3
Discoid Core-Edge Flake	SMR-1W	2	41.2	44.5	47.7
Flake	SMR-1	30	8.8	21.9	52.1
Flake	SMR-1E	5	14.2	22.7	41.6
Flake	SMR-1W	12	11.2	23.9	80.7
Kombewa Flake	SMR-1	25	8.0	14.0	37.7
Kombewa Flake	SMR-1E	5	12.0	38.2	40.2
Kombewa Flake	SMR-1W	8	10.6	20.3	68.6
Levallois Recurrent Flake	SMR-1	50	20.5	35.0	82.9
Levallois Recurrent Flake	SMR-1E	15	25.1	39.7	88.9
Levallois Recurrent Flake	SMR-1W	40	17.0	37.6	79.4
Overshot Flake	SMR-1	27	14.4	40.4	109.1
Overshot Flake	SMR-1E	5	23.3	31.3	87.9
Overshot Flake	SMR-1W	15	15.8	26.5	77.0
Width					
Core-Edge Flake	SMR-1	44	9.6	27.4	90.4
Core-Edge Flake	SMR-1E	18	15.0	25.2	76.1
Core-Edge Flake	SMR-1W	31	12.6	32.4	78.8
Cortical Flake	SMR-1	11	15.9	27.2	47.4
Cortical Flake	SMR-1E	8	15.6	30.4	58.7
Cortical Flake	SMR-1W	8	26.8	38.8	53.5
Discoid Centripetal Flake	SMR-1	5	27.6	36.5	52.4
Discoid Centripetal Flake	SMR-1E	4	21.1	32.1	45.9
Discoid Centripetal Flake	SMR-1W	4	20.1	31.8	40.3
Discoid Core-Edge Flake	SMR-1	6	22.5	28.5	32.7
Discoid Core-Edge Flake	SMR-1E	3	26.8	30.4	40.8
Discoid Core-Edge Flake	SMR-1W	2	29.9	38.5	47.1
Flake	SMR-1	30	7.2	19.9	61.7
Flake	SMR-1E	5	19.4	24.2	39.9
Flake	SMR-1W	12	12.6	22.3	73.4
Kombewa Flake	SMR-1	25	9.3	16.1	45.4
Kombewa Flake	SMR-1E	5	10.5	32.1	48.7
Kombewa Flake	SMR-1W	8	14.4	20.6	50.8
Levallois Recurrent Flake	SMR-1	50	12.7	25.4	79.8
Levallois Recurrent Flake	SMR-1E	15	13.7	25.5	51.9
Levallois Recurrent Flake	SMR-1W	40	10.9	28.6	74.3
Overshot Flake	SMR-1	27	15.8	28.4	61.2
Overshot Flake	SMR-1E	5	20.3	25.1	39.3
Overshot Flake	SMR-1W	15	12.8	22.7	67.8
Thickness					
Core-Edge Flake	SMR-1	44	4.4	8.2	18.2
Core-Edge Flake	SMR-1E	18	6.2	10.5	18.5
Core-Edge Flake	SMR-1W	31	3.8	8.0	42.6

Table 13 (continued)

Type	Assemblage	*N*	Min.	Median	Max.
Cortical Flake	SMR-1	11	4.5	8.4	11.2
Cortical Flake	SMR-1E	8	3.5	8.6	25.9
Cortical Flake	SMR-1W	8	6.4	11.2	21.4
Discoid Centripetal Flake	SMR-1	5	8.1	12.6	19.0
Discoid Centripetal Flake	SMR-1E	4	5.1	8.4	16.7
Discoid Centripetal Flake	SMR-1W	4	6.7	8.7	14.1
Discoid Core-Edge Flake	SMR-1	6	9.5	11.1	13.0
Discoid Core-Edge Flake	SMR-1E	3	8.8	13.4	13.7
Discoid Core-Edge Flake	SMR-1W	2	14.9	17.5	20.1
Flake	SMR-1	30	0.9	4.4	12.7
Flake	SMR-1E	5	4.3	4.9	9.5
Flake	SMR-1W	12	2.9	5.4	19.4
Kombewa Flake	SMR-1	25	1.6	3.3	13.3
Kombewa Flake	SMR-1E	5	2.5	8.8	10.0
Kombewa Flake	SMR-1W	8	2.3	4.5	10.8
Levallois Recurrent Flake	SMR-1	50	2.3	5.5	24.5
Levallois Recurrent Flake	SMR-1E	15	3.9	5.6	10.7
Levallois Recurrent Flake	SMR-1W	40	2.0	5.8	15.4
Overshot Flake	SMR-1	27	3.1	8.8	15.7
Overshot Flake	SMR-1E	5	3.9	4.2	12.2
Overshot Flake	SMR-1W	15	3.2	6.2	25.1
Mean Thickness					
Core-Edge Flake	SMR-1	40	4.5	8.2	17.1
Core-Edge Flake	SMR-1E	18	6.2	9.5	18.8
Core-Edge Flake	SMR-1W	29	5.0	7.6	33.9
Discoid Centripetal Flake	SMR-1	5	6.9	11.8	19.2
Discoid Centripetal Flake	SMR-1E	3	6.8	9.9	13.6
Discoid Centripetal Flake	SMR-1W	4	6.7	8.2	13.4
Discoid Core-Edge Flake	SMR-1	6	9.5	10.6	13.9
Discoid Core-Edge Flake	SMR-1E	3	8.8	11.6	13.6
Discoid Core-Edge Flake	SMR-1W	2	12.1	13.9	15.7
Levallois Recurrent Flake	SMR-1	43	3.9	5.6	24.0
Levallois Recurrent Flake	SMR-1E	15	4.1	6.3	10.4
Levallois Recurrent Flake	SMR-1W	37	1.9	6.0	15.9
Overshot Flake	SMR-1	24	3.0	8.9	13.2
Overshot Flake	SMR-1E	5	3.9	4.2	11.3
Overshot Flake	SMR-1W	11	3.5	8.2	21.0

Palaeolithic. The rockshelter is located in Epirus, west of the Pindos range (Fig. 1, n. 11). The site was excavated between 1964 and 1966 (Bailey et al., 1992; Higgs & Vita-Finzi, 1966; Papaconstantinou, 1989). The inner part of the rockshelter revealed an in-situ deposit consisting of a 5 m deep sequence comprising 30 levels (Higgs & Vita-Finzi, 1966). New excavations were conducted in the 1980s, which have led to a new interpretation of the sequence with fewer levels (Bailey et al., 1992). Moreover, within the rockshelter the deposit is divided between the external and the internal part, and the internal part is divided into the eastern and western areas (Papaconstantinou, 1989). Hence, while the 1966 sequence reports a Gravettian layer in level 9, an occupation hiatus in level 14, and Middle Palaeolithic occupations from level 15 to 30, the 1983 relabelled the level 9 as layer 10, the level 14 as layer 13 and the Middle Palaeolithic occupations extend from layer 14 to 19 (Papaconstantinou, 1989). While the radiocarbon dates from the site present some problems, especially those of the upper Middle Palaeolithic deposits, the thermoluminescence dates from the lowest layers show a certain consistency around 100 ka BP (Table 18; Bailey et al., 1992; Papaconstantinou, 1989).

The upper Mousterian levels (15–23, 1966 excavations; 14, 1983 excavations) were attributed to the Micromousterian, characterised by general small dimensions, "crude", retouch, and several pointed artefacts, while the lower Mousterian levels (24–30, 1966 excavations; 16–18, 1983 excavations) were named Basal Mousterian and consisting of larger and elongated blanks, with much more platform facetting, Levallois centripetal cores, and finer retouched

Table 14 Internal platform angle (IPA) and external platform angle (EPA) minimum, median, and maximum values (degrees) in blank categories across assemblages. Only complete blanks bigger than 39.99 mm in linear size (combined length and width)

Type	Site	*N*	Min.	Median	Max.
IPA					
Core-Edge Flake	SMR-1	40	85	110	135
Core-Edge Flake	SMR-1E	18	90	110	135
Core-Edge Flake	SMR-1W	29	85	105	120
Cortical Flake	SMR-1	9	95	107.5	115
Cortical Flake	SMR-1E	7	80	112.5	120
Cortical Flake	SMR-1W	8	95	105	125
Discoid Centripetal Flake	SMR-1	5	115	115	125
Discoid Centripetal Flake	SMR-1E	3	100	100	125
Discoid Centripetal Flake	SMR-1W	4	105	107.5	125
Discoid Core-Edge Flake	SMR-1	6	100	107.5	115
Discoid Core-Edge Flake	SMR-1E	3	105	105	115
Discoid Core-Edge Flake	SMR-1W	2	105	105	105
Flake	SMR-1	18	85	100	120
Flake	SMR-1E	4	100	107.5	110
Flake	SMR-1W	7	90	105	105
Kombewa Flake	SMR-1	9	85	100	105
Kombewa Flake	SMR-1E	4	110	115	120
Kombewa Flake	SMR-1W	4	100	107.5	115
Levallois Recurrent Flake	SMR-1	43	85	100	120
Levallois Recurrent Flake	SMR-1E	15	95	105	115
Levallois Recurrent Flake	SMR-1W	37	80	105	120
Overshot Flake	SMR-1	24	95	110	130
Overshot Flake	SMR-1E	5	95	105	120
Overshot Flake	SMR-1W	11	95	107.5	130
EPA					
Core-Edge Flake	SMR-1	40	50	75	90
Core-Edge Flake	SMR-1E	18	45	70	90
Core-Edge Flake	SMR-1W	29	60	75	90
Cortical Flake	SMR-1	9	55	70	95
Cortical Flake	SMR-1E	7	50	60	80
Cortical Flake	SMR-1W	8	45	77.5	85
Discoid Centripetal Flake	SMR-1	5	55	60	60
Discoid Centripetal Flake	SMR-1E	3	50	60	75
Discoid Centripetal Flake	SMR-1W	4	55	65	70
Discoid Core-Edge Flake	SMR-1	6	55	70	85
Discoid Core-Edge Flake	SMR-1E	3	60	70	70
Discoid Core-Edge Flake	SMR-1W	2	75	77.5	80
Flake	SMR-1	18	45	75	90
Flake	SMR-1E	4	60	67.5	75
Flake	SMR-1W	7	60	72.5	80
Kombewa Flake	SMR-1	9	65	75	90
Kombewa Flake	SMR-1E	4	60	60	60
Kombewa Flake	SMR-1W	4	60	65	70
Levallois Recurrent Flake	SMR-1	43	60	75	95
Levallois Recurrent Flake	SMR-1E	15	65	70	85
Levallois Recurrent Flake	SMR-1W	37	60	75	90
Overshot Flake	SMR-1	24	55	75	90
Overshot Flake	SMR-1E	5	60	80	85
Overshot Flake	SMR-1W	11	65	70	85

endscrapers (Higgs & Vita-Finzi, 1966). Any technological change cannot be attributed to a different raw material procurement, as the Asprochaliko Mousterian exploited pebbles collected from the neighbouring Louros Gorge (Ligkovanlis, 2016; Papaconstantinou, 1989). Papaconstantinou reanalysed part of the Middle Palaeolithic assemblage coming from the upper and lower Mousterian layers (Papaconstantinou, 1989). The author reports a mostly unidirectional recurrent Levallois method in layer 18, with some centripetal modality. Layer 16 is rather difficult to assign, as most of the artefacts are fragmented, there are fewer cores, and most of the blanks are undiagnostic. Nevertheless, in its upper part, there are several core-edge flakes and pseudo-Levallois points. Layer 14 shows a technological change, as most of the flakes have plain platforms and the pseudo-Levallois points, together with core-edge flakes, are numerous. The cores are mostly on flakes and exploited centripetally. The author concludes that the reduction method was rather secant and conducted from a single striking platform. For the production of the pseudo-Levallois points, he conceives a reduction method, named the Asprochaliko method, which is applied to the flakes obtained by orthogonal secant reduction (Bailey et al., 1992; Papaconstantinou, 1989). The same method can be applied to nodules. In both cases, there is an element of predetermination to obtain the pseudo-Levallois point or the core-edge flake. The Asprochaliko method is essentially a Kombewa method on the ventral face of the former flake. Therefore, the Asprochaliko Middle Palaeolithic stratigraphic sequence identifies a frankly Levallois recurrent industry in the lower layers, while the upper layers are characterised by a more secant reduction method aimed at thicker blanks. Nevertheless, to find analogies, Papaconstantinou aligned the Asprochaliko method within the Levallois recurrent centripetal modality (Ligkovanlis, 2016; Papaconstantinou, 1989). Subsequent analyses did not clarify whether the upper Mousterian layers' technology lies more in the discoidal or Levallois realm (Ligkovanlis, 2016). The latest analysis (2012) retrieved samples from the whole sequence (Ligkovanlis, 2016). The new findings radically changed the technological interpretation as the lower layers have a non-Levallois component, mainly discoidal and core-on-flake (Kombewa) methods, aimed to produce pseudo-Levallois points (Ligkovanlis, 2016). Also, the elongated blanks and the absence of recurrent Levallois cores do not support assigning the lower layers mostly to a Levallois-based reduction (Ligkovanlis, 2016). Furthermore, the Asprochaliko method has now been recognised as a variant within the discoidal methods (Ligkovanlis, 2016). To sum up, the Asprochaliko Middle Palaeolithic assemblages are more technologically uniform than previously

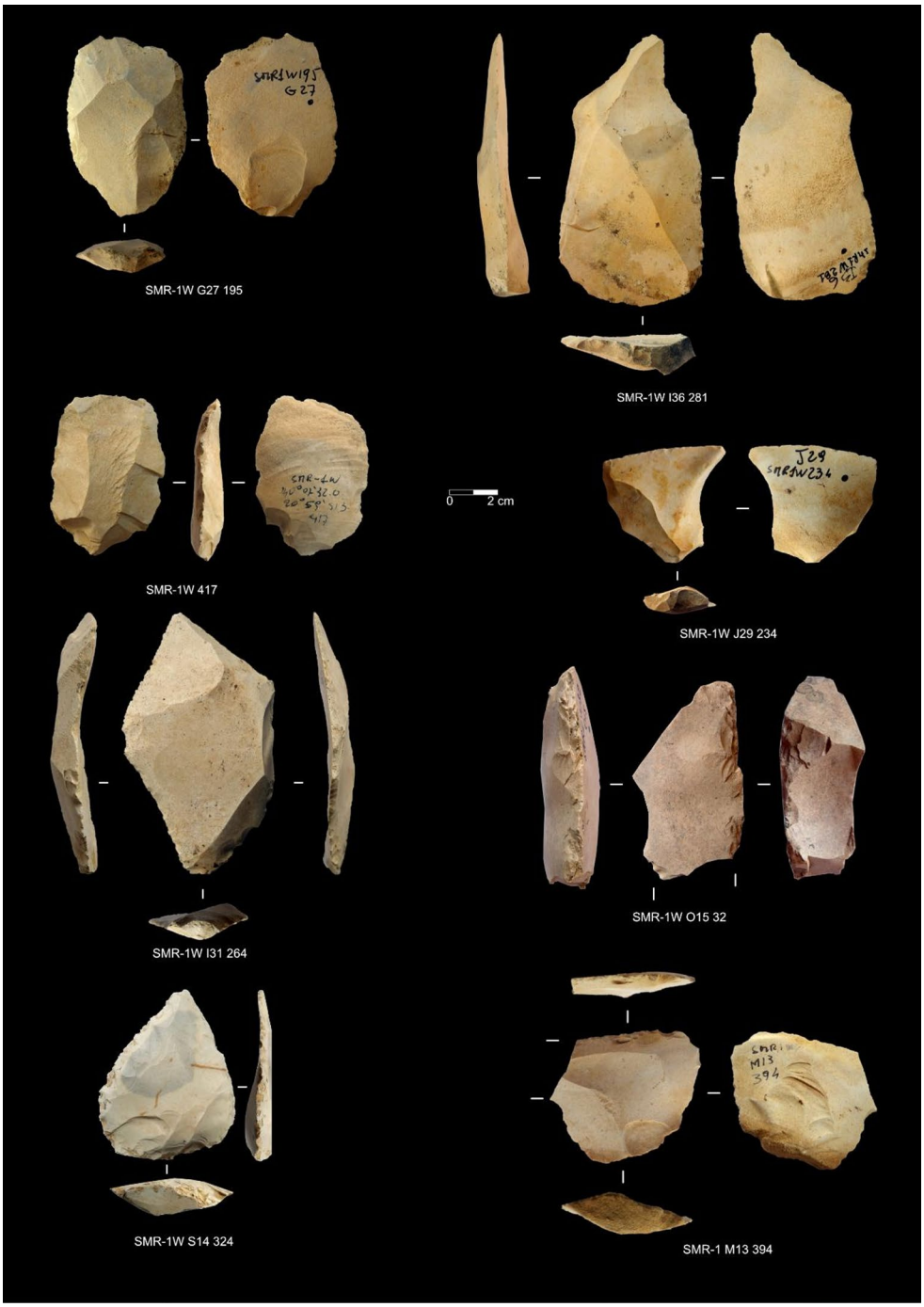

Fig. 10 Retouched artefacts. Convex sidescraper: SMR-1W G27 195, double rectilinear sidescraper: SMR-1W I36 281, alternated sidescraper with basal thinning: SMR-1W 417, transversal sidescraper: SMR-1W J29 234, SMR-1 M13 394, simple convex sidescraper: SMR-1W I31 264, simple rectilinear sidescraper: SMR-1W O15 32, Mousterian point: SMR-1W S14 324. (Photographs by Elisabetta Starnini)

thought. Analogies between SMR1 and Asprochaliko can be drawn on the centripetal, mostly on a single surface, reduction that is found in both assemblages. Moreover, the knapping on ventral faces is a common characteristic.

Kokkinopilos

Kokkinopilos is an open-air site located a few kilometres from Asprochaliko (Fig. 1, n. 34). Lithic artefacts have been found eroded or embedded in *terra rossa* soils (Dakaris et al., 1964; Higgs & Vita-Finzi, 1966; Papagianni, 1999, 2000; Tourloukis et al., 2015). The site was discovered in 1962 during a survey carried out in the Epirote landscape (Dakaris et al., 1964). Noticing embedded artefacts and artefact scatters next to gully profiles, stratigraphic investigations were carried out in site α and site β, where three main soil depositions were defined (A, B, C – from lower to top). Middle Palaeolithic artefacts have been found embedded at the base of zone B (Dakaris et al., 1964). Further geoarchaeological research at Kokkinopilos suggested either a

Table 15 Retouched artefacts from the assemblages grouped by technological types, classified according to F. Bordes' typological list (Bordes, 1961)

Categories	SMR-1		SMR-1E		SMR-1W		Total	
	N	%	*N*	%	*N*	%	*N*	%
Levallois Recurrent Flake		**0.0**		**0.0**	**7**	**30.4**	**7**	**25.0**
10 - simple convex scraper		0.0		0.0	1	4.3	1	3.6
12 - double simple rectilinear scraper		0.0		0.0	1	4.3	1	3.6
29 - alternated scraper		0.0		0.0	1	4.3	1	3.6
42 - notch		0.0		0.0	1	4.3	1	3.6
43 - denticulate		0.0		0.0	1	4.3	1	3.6
6 - Mousterian point		0.0		0.0	1	4.3	1	3.6
9 - simple rectilinear scraper		0.0		0.0	1	4.3	1	3.6
Flake	**2**	**50.0**		**0.0**	**4**	**17.4**	**6**	**21.4**
12 - double simple rectilinear scraper		0.0		0.0	2	8.7	2	7.1
18 - convergent rectilinear scraper		0.0		0.0	1	4.3	1	3.6
22 - transversal rectilinear scraper		0.0		0.0	1	4.3	1	3.6
9 - simple rectilinear scraper	2	50.0		0.0		0.0	2	7.1
Core-Edge Flake	**1**	**25.0**		**0.0**	**4**	**17.4**	**5**	**17.9**
10 - simple convex scraper		0.0		0.0	2	8.7	2	7.1
22 - transversal rectilinear scraper		0.0		0.0	1	4.3	1	3.6
23 - convex transversal scraper	1	25.0		0.0		0.0	1	3.6
9 - simple rectilinear scraper		0.0		0.0	1	4.3	1	3.6
Overshot Flake		**0.0**		**0.0**	**3**	**13.0**	**3**	**10.7**
22 - transversal rectilinear scraper		0.0		0.0	1	4.3	1	3.6
9 - simple rectilinear scraper		0.0		0.0	1	4.3	1	3.6
9 - simple straight scraper		0.0		0.0	1	4.3	1	3.6
Levallois Preferential Flake		**0.0**		**0.0**	**2**	**8.7**	**2**	**7.1**
22 - transversal rectilinear scraper		0.0		0.0	2	8.7	1	7.1
Kombewa Flake		**0.0**		**0.0**	**2**	**8.7**	**2**	**7.1**
42 - notch		0.0		0.0	1	4.3	1	3.6
9 - simple straight scraper		0.0		0.0	1	4.3	1	3.6
Levallois Blade		**0.0**	**1**	**100.0**	**1**	**4.3**	**2**	**7.1**
45 - flakes with retouch on the ventral surface		0.0	1	100.0		0.0	1	3.6
9 - simple rectilinear scraper		0.0		0.0	1	4.3	1	3.6
Predetermining Flake	**1**	**25.0**		**0.0**		**0.0**	**1**	**3.6**
43 - denticulate	1	25.0		0.0		0.0	1	3.6
Total	**4**	**100.0**	**1**	**100.0**	**23**	**100.0**	**28**	**100.0**

complete reworking of the sediments (Bailey et al., 1992) or a complex sedimentary evolution involving the formation of paleosols and their progressive exposition (van Andel, 1998). The topmost paleosol in Kokkinopilos has been dated to 91 ± 14 ka by thermoluminescence (Zhou et al., 2000). New research carried out at the site revisited the sequence studied by van Andel and Runnells. It led to the discovery of embedded handaxes and other lithic artefacts and concluded that the sediment under the topmost paleosol is older than 172 ± 25 ka and 206 ± 19 ka (Tourloukis et al., 2015). This research provided new data; while concluding that lithic artefacts are likely in situ in a Middle Pleistocene sediment, it is unclear whether they are pristine subaerial accumulation or more likely to be palimpsests in waterlogged conditions (Tourloukis et al., 2015).

Most of the artefacts retrieved from Kokkinopilos have been attributed to the Middle Palaeolithic. There is an occurrence of the Levallois method and also bifacially retouched tools associated with the Micoquian or Keilmessergruppen technological tradition (Dakaris et al., 1964; Tourloukis et al., 2015). D. Papagianni provided a detailed analysis of site α and site β assemblages within her reanalysis of northwestern Greece open-air Middle Palaeolithic surface scatters (Papagianni, 1999, 2000). She found that site β mostly shows unidirectional and convergent reductions, which correspond to Levallois and prismatic cores; the centripetal reductions, either Levallois or discoid, are rarely represented. The modified blanks included mostly sidescrapers and Levallois points on unidirectional or convergent blanks, and there are also three bifacial points (Papagianni, 2000). Site α, despite having a larger assemblage, is rather undiagnostic because the artefacts are mostly knapping debris and there is a large component of Upper Palaeolithic (Gravettian) artefacts. Results for the

Fig. 11 Artefacts made of other raw materials than local siliceous limestone. Grey chert: SMR-1E GG104 849, SMR-1 M9 261, SMR-1 N7 427. Vasilitsa green chert: SMR-1W I29 241. Grey radiolarite: SMR-1 N4 385, SMR-1W L26 442. Red radiolarite: SMR-1W P12 318, SMR-1W J25 131, SMR-1 G9 2101, SMR-1 M12 345, SMR-1 L14 373, SMR-1E AH110 2220, SMR-1 O12 3070, SMR-1 P12 793. Quartz: SMR-1W Q19 279, SMR-1 G5 8. (Photographs by Elisabetta Starnini)

Mousterian diagnostic lithics are mostly akin to those of site β, but without bifacial points (Papagianni, 2000).

Theopetra

Theopetra is a cave site in Thessaly, east of the Pindos Range (Fig. 1, n. 140). The long sequence spans from historic times to the Middle Palaeolithic (Darlas, 2007; Facorellis et al., 2013; Karkanas, 1999). As in most caves, the deposition is complex and involves events of burrowing and erosion. The Middle Palaeolithic is found in unit (Episode) II, which consists of twelve layers (Karkanas, 1999). Unit II is a water-lain sediment interrupted by burnt layers; the most discernible layers are II2, II4, II6, and II11 (Karkanas, 1999). In addition to lithic assemblages, footprints in layer II2 belonging to a Neanderthal child show the human presence in the cave during the Middle Palaeolithic (Kyparissi-Apostolika, 1999; Kyparissi-Apostolika & Manolis, 2021; Panagopoulou, 1999). Attempts to date the Middle Palaeolithic deposit have been made through radiocarbon, thermoluminescence, and tephrachronology; the latter two methods provided the likeliest dating (Facorellis et al., 2013; Karkanas et al., 2015; Karkanas & Kyparissi-Apostolika, 2024; Kyparissi-Apostolika & Manolis, 2021; Valladas et al., 2007). Thermoluminescence on burnt lithic artefacts dated layer II2 to 124 ± 16 ka and II4 to 129 ± 13 ka, placing them at the transition between MIS 6 and 5 (Valladas et al., 2007). Layer II11, attributed to the Upper Palaeolithic based on scant lithic artefacts, has been dated to 57 ± 6 ka (Facorellis et al., 2013; Valladas et al., 2007). Cryptotephra analysis shows that layer II11 is bracketed between > 50 ka and 45.7 ka, while the

Table 16 Artefacts divided by raw material across the assemblages and their relative frequencies amongst categories (Blades, Bladelets, Cores, Flakes, Fragments) and technological types

Categories	SMR-1		SMR-1E		SMR-1W		SMR1-exc		Total	
	N	%	*N*	%	*N*	%	*N*	%	*N*	%
Siliceous Limestone	**1023**	94.5	260	97.4	445	96.4	5	100.0	1733	**95.4**
Blades	**51**	**5.0**	**14**	**5.4**	**19**	**4.2**		**0.0**	**84**	**4.8**
Levallois Recurrent Flake	17	33.3	3	21.4	3	16.7			23	27.7
Levallois Blade	11	21.6	2	14.3	8	44.4			21	25.3
Core-Edge Flake	9	17.6	7	50.0	3	11.1			19	21.7
Overshot Flake	8	15.7	1	7.1	3	16.7			12	14.5
Predetermining Flake	3	5.9		0.0	1	5.6			4	4.8
Blade	1	2.0	1	7.1		0.0			2	2.4
Kombewa Flake	1	2.0		0.0	1	5.6			2	2.4
Cortical Flake	1	2.0		0.0		0.0			1	1.2
Bladelets	**9**	**0.9**	**3**	**1.2**	**2**	**0.5**		**0.0**	**14**	**0.8**
Predetermining Flake	6	66.7	1	33.3		0.0			7	50.0
Bladelet	1	11.1	2	66.7	2	100.0			5	35.7
Levallois Recurrent Flake	2	22.2		0.0		0.0			2	14.3
Cores	**18**	**1.8**	**12**	**4.6**	**16**	**3.3**		**0.0**	**46**	**2.6**
Levallois	11	61.1	6	50.0	9	50.0			26	54.5
Hierarchical Discoid	4	22.2	3	25.0	3	21.4			10	22.7
Expedient		0.0	1	8.3	2	14.3			3	6.8
SSDA	2	11.1		0.0		0.0			2	4.5
Discoid	1	5.6		0.0	1	7.1			2	4.5
Levallois and Hierarchical Discoid		0.0	1	8.3		0.0			1	2.3
Centripetal		0.0	1	8.3		0.0			1	2.3
Prismatic		0.0		0.0	1	7.1			1	2.3
Flakes	**705**	**68.9**	**191**	**73.5**	**355**	**80.1**	**4**	**80.0**	**1255**	**72.4**
Flake	318	45.1	65	34.0	104	30.1	3	75.0	490	39.4
Levallois Recurrent Flake	83	11.8	37	19.4	81	22.2		0.0	201	15.8
Predetermining Flake	91	12.9	17	8.9	46	12.9	1	25.0	155	12.3
Kombewa Flake	91	12.9	25	13.1	21	5.8		0.0	137	11.0
Core-Edge Flake	48	6.8	15	7.9	48	13.7		0.0	111	8.9
Overshot Flake	29	4.1	6	3.1	19	5.3		0.0	54	4.3
Cortical Flake	16	2.3	13	6.8	10	2.6		0.0	39	3.1
Pseudo-Levallois point	11	1.6	3	1.6	9	2.6		0.0	23	1.9
Discoid Centripetal Flake	8	1.1	5	2.6	6	1.8		0.0	19	1.5
Levallois Preferential Flake	3	0.4	1	0.5	8	2.3		0.0	12	1.0
Discoid Core-Edge Flake	6	0.9	2	1.0	1	0.0		0.0	9	0.6
Levallois Blade		0.0	1	0.5	2	0.6		0.0	3	0.2
Crest	1	0.1		0.0		0.0		0.0	1	0.1
Levallois point		0.0	1	0.5		0.0		0.0	1	0.1
Fragments	**240**	**23.5**	**40**	**15.4**	**53**	**11.9**	**1**	**20.0**	**334**	**19.4**
Radiolarite	**31**	**2.9**	**3**	**1.1**	**5**	**1.1**		**0.0**	**39**	**2.2**
Blades		**0.0**	**1**	**33.3**	**2**	**40.0**			**3**	**7.7**
Core-Edge Flake			1	100.0	1	50.0			2	66.7
Levallois Blade				0.0	1	50.0			1	33.3
Flakes	**22**	**71.0**	**1**	**33.3**	**3**	**60.0**			**26**	**66.7**
Flake	10	45.5	1	100.0	2	66.7			13	50.0
Levallois Recurrent Flake	3	13.6		0.0	1	33.3			4	15.4
Predetermining Flake	3	13.6		0.0		0.0			3	11.5
Overshot Flake	2	9.1		0.0		0.0			2	7.7
Core-Edge Flake	2	9.1		0.0		0.0			2	7.7
Kombewa Flake	1	4.5		0.0		0.0			1	3.8
Levallois Preferential Flake	1	4.5		0.0		0.0			1	3.8
Fragments	**9**	**29.0**	**1**	**33.3**		**0.0**			**10**	**25.6**
Grey Chert	**10**	**0.9**		**0.0**	**2**	**0.5**		**0.0**	**12**	**0.7**

Table 16 (continued)

Categories	SMR-1		SMR-1E		SMR-1W		SMR1-exc		Total	
	N	%	*N*	%	*N*	%	*N*	%	*N*	%
Flakes	**7**	**70.0**			**1**	**50.0**			**8**	**66.7**
Flake	4	57.1			1	100.0			5	62.5
Levallois Recurrent Flake	2	28.6				0.0			2	25.0
Overshot Flake	1	14.3				0.0			1	12.5
Fragments	**3**	**30.0**			**1**	**50.0**			**4**	**33.3**
Other raw materials	**5**	**0.5**		**0.0**	**2**	**0.5**		**0.0**	**7**	**0.4**
Blades	**2**	**40.0**				**0.0**			**2**	**28.6**
Blade	2	100.0							2	100.0
Flakes	**3**	**60.0**			**1**	**50.0**			**4**	**57.1**
Flake	3	100.0			1	100.0			4	100.0
Fragments		**0.0**			**1**	**50.0**			**1**	**14.3**
Green Chert	**2**	**0.2**	**2**	**0.0**	**4**	**0.9**		**0.0**	**8**	**0.3**
Blades		**0.0**	**1**			**0.0**			**1**	**0.0**
Levallois Recurrent			1						1	
Flake	**2**	**100.0**	**1**		**4**	**100.0**			**7**	**100.0**
Flake	2	100.0			1	25.0			3	50.0
Levallois Recurrent Flake		0.0			2	50.0			2	33.3
Core-Edge Flake		0.0	1		1	25.0			2	16.7
Quartz	**4**	**0.4**		**0.0**	**1**	**0.2**		**0.0**	**5**	**0.3**
Flakes	**2**	**50.0**			**1**	**100.0**			**3**	**60.0**
Flake	2	100.0				0.0			2	66.7
Overshot Flake		0.0			1	100.0			1	33.3
Fragments	**2**	**50.0**				**0.0**			**2**	**40.0**
Grey Radiolarite	**1**	**0.1**	**1**	**0.4**	**1**	**0.2**		**0.0**	**3**	**0.2**
Flakes	**1**	**100.0**	**1**	**100.0**	**1**	**100.0**			**3**	**100.0**
Cortical Flake	1	100.0		0.0		0.0			1	33.3
Levallois Recurrent Flake		0.0		0.0	1	100.0			1	33.3
Flake		0.0	1	100.0		0.0			1	33.3
Grey radiolarite	**2**	**0.2**		**0.0**		**0.0**		**0.0**	**2**	**0.1**
Flakes	**1**	**50.0**							**1**	**50.0**
Predetermining Flake	1	100.0							1	100.0
Fragments	**1**	**50.0**							**1**	**50.0**
Brown chert	**1**	**0.1**	**1**	**0.4**		**0.0**		**0.0**	**2**	**0.1**
Flakes	**1**	**100.0**	**1**	**100.0**					**2**	**100.0**
Flake	1	100.0		0.0					1	50.0
Discoid Core-Edge Flake		0.0	1	100.0					1	50.0
Grey Chert	**1**	**0.1**	**3**	**0.4**		**0.0**		**0.0**	**4**	**0.1**
Blades		**0.0**	**1**	**0.0**					**1**	**0.0**
Levallois Blade			1						1	
Cores		**0.0**	**1**	**0.0**					**1**	**0.0**
Prismatic			1						1	
Flakes	**1**	**100.0**	**1**	**100.0**					**2**	**100.0**
Cortical Flake	1	100.0		0.0					1	50.0
Core-Edge Flake		0.0	1	100.0					1	50.0
Silicified Breccia	**1**	**0.1**		**0.0**		**0.0**		**0.0**	**1**	**0.1**
Fragments	**1**	**100.0**							**1**	**100.0**
Brown radiolarite	**1**	**0.1**		**0.0**		**0.0**		**0.0**	**1**	**0.1**
Flakes	**1**	**100.0**							**1**	**100.0**
Predetermining Flake	1	100.0							1	100.0
Quartzite		**0.0**		**0.0**	**1**	**0.2**		**0.0**	**1**	**0.1**
Flakes					**1**	**100.0**			**1**	**100.0**
Discoid Core-Edge Flake					1	100.0			1	100.0
Grey Blue chert		**0.0**	**1**	**0.4**		**0.0**		**0.0**	**1**	**0.1**

Table 16 (continued)

Categories	SMR-1		SMR-1E		SMR-1W		SMR1-exc		Total	
	N	%	*N*	%	*N*	%	*N*	%	*N*	%
Fragments			**1**	**100.0**					**1**	**100.0**
Total	**1082**	**100.0**	**271**	**100.0**	**461**	**100.0**	**5**	**100.0**	**1819**	**100.0**

Fig. 12 Nodules of raw material from Delichmét - Mt. Kirkouri watershed, photographed in 2023. The calliper's lines measure up to 17 cm (Photographs by Jacopo Gennai)

Fig. 13 Siliceous boulder nearly 600 mm long found on Mt. Kirkouri slopes (Photograph by Paolo Biagi)

interface between layers II4 and II5 might coincide with a 128–131 ka age, therefore in alignment with the thermoluminescence dates (Karkanas et al., 2015). The Middle Palaeolithic lithic assemblages from Theopetra have been attributed to the Quina method in the lower part of the sequence, and to the Levallois in the middle and upper parts (Panagopoulou, 1999). The raw material is mostly radiolarite coming from the Koziakias-Pindos range (Karkanas et al., 2008; Panagopoulou, 1999). The Levallois is mostly recurrent centripetal, though there is a laminar component (Panagopoulou, 1999). In general, the lithic artefacts in Theopetra have small dimensions due to the intense reduction activity on medium to long-distance raw material (Karkanas et al., 2008; Panagopoulou, 1999).

Dalani i Vogël

Dalani i Vogël is part of a complex of findspots along the coast of southern Albania (Ruka et al., 2014) (Fig. 1, n. 1). The site has an exposed profile due to water erosion of a manmade channel and sea action (Badino et al., 2025). Section 2/A yielded Middle Palaeolithic artefacts embedded in a massive silty clay Unit a, and in the overlaying sandy silty Unit b (Badino et al., 2025). Luminescence dates of these units are 42.9 ± 1.5 ka (Unit a) and 38.7 ± 1.4 ka (Unit b) (Badino et al., 2025).

The few artefacts found embedded in the stratigraphic units are complemented by surface finds, which are mostly attributed to the Middle Palaeolithic (Badino et al., 2025). The lithic technology is characterised by a Levallois recurrent centripetal reduction, using small pebbles. Cores and products that do not exhibit all the characteristics of Levallois knapping likely follow a centripetal surface knapping (Badino et al., 2025).

Fig. 14 Large cores preserving a large portion of the original nodule shape from SMR-1 and la Greklu ridge (Photographs by Elisabetta Starnini)

The Evidence from Undated Sites in Neighbouring Areas

In addition to the stratified sites, it is important to include in the overview the major unstratified or buried but reworked assemblages that have been attributed to the Middle Palaeolithic.

Agia

The site was discovered in the Preveza area during the Nikopolis project survey (Fig. 1, n. 12; Runnels & van Andel, 2003). The most recognisable technology is the Levallois recurrent centripetal method or a generic centripetal flaking (Papagianni, 2000; Spathas, 2023). The data from

Table 17 Pairwise statistical comparisons of external (EPA) and internal (IPA) platform angles between blanks from known discoid, hierarchical discoid, and centripetal Levallois experimental knapping (Bustos) and SMR1 ones

Bustos-Peréz experimental blanks	SMR1 blanks	statistic	*p*. value	*p*. adjust method	test
EPA					
Bustos Hierarchical Discoid Backed Flake	SMR1 Levallois Recurrent Flake	6.364525	2.66E-08	Holm	Dunn
Bustos Discoid Flake	SMR1 Levallois Recurrent Flake	6.319838	3.53E-08	Holm	Dunn
Bustos Discoid Backed Flake	SMR1 Levallois Recurrent Flake	5.747502	1.21E-06	Holm	Dunn
Bustos Hierarchical Discoid Flake	SMR1 Levallois Recurrent Flake	4.940395	0.000103	Holm	Dunn
Bustos Hierarchical Discoid Backed Flake	SMR1 Flake	4.837229	0.000171	Holm	Dunn
Bustos Discoid Flake	SMR1 Flake	4.598213	0.000545	Holm	Dunn
Bustos Discoid Backed Flake	SMR1 Flake	4.58716	0.000571	Holm	Dunn
Bustos Hierarchical Discoid Flake	SMR1 Flake	3.768054	0.020072	Holm	Dunn
Bustos Hierarchical Discoid Backed Flake	SMR1 Core-Edge Flake	3.763273	0.020292	Holm	Dunn
IPA					
Bustos Hierarchical Discoid Backed Flake	SMR1 Levallois Recurrent Flake	6.364525	2.66E-08	Holm	Dunn
Bustos Discoid Flake	SMR1 Levallois Recurrent Flake	6.319838	3.53E-08	Holm	Dunn
Bustos Discoid Backed Flake	SMR1 Levallois Recurrent Flake	5.747502	1.21E-06	Holm	Dunn
Bustos Hierarchical Discoid Flake	SMR1 Levallois Recurrent Flake	4.940395	0.000103	Holm	Dunn
Bustos Hierarchical Discoid Backed Flake	SMR1 Flake	4.837229	0.000171	Holm	Dunn
Bustos Discoid Flake	SMR1 Flake	4.598213	0.000545	Holm	Dunn
Bustos Discoid Backed Flake	SMR1 Flake	4.58716	0.000571	Holm	Dunn
Bustos Hierarchical Discoid Flake	SMR1 Flake	3.768054	0.020072	Holm	Dunn
Bustos Hierarchical Discoid Backed Flake	SMR1 Core-Edge Flake	3.763273	0.020292	Holm	Dunn

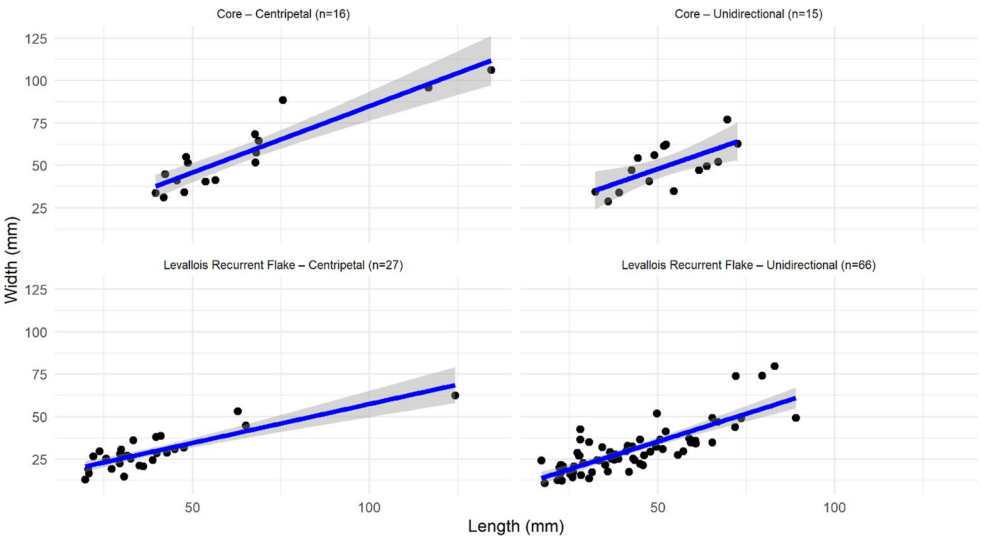

Fig. 15 Scatterplot of length and width in complete Levallois recurrent flakes and cores having unidirectional and centripetal scar patterns and Spearman correlations. Produced in R (R Core Team, 2025) with the ggstatsplot package (Patil, 2021) by Jacopo Gennai

Table 18 Radiometric dates from Asprochaliko

Layer/level	Date ID	Date	Error	Method	Technocomplex attribution	Reference
9	I.1965	26,100	900	Radiocarbon	Upper Palaeolithic (Gravettian)	(Higgs & Vita-Finzi, 1966)
19	I.1957	>39,900		Radiocarbon	Middle Palaeolithic (Micromousterian)	(Higgs & Vita-Finzi, 1966)
18	?	102,000	14,000	Thermoluminescence on flint	Middle Palaeolithic (Basal Mousterian)	(Papaconstantinou, 1989)
18	OxTL299	98,500	12,000	Thermoluminescence on flint	Middle Palaeolithic (Basal Mousterian)	(Bailey et al., 1992)

the unretouched blanks attest to some unidirectional flaking too (Papagianni, 2000).

Alonaki

The site was discovered in the Preveza area during the Nikopolis project survey (Fig. 1, n. 4; Runnels & van Andel, 2003). While the Levallois method is used in its recurrent centripetal and preferential modalities, most of the cores attest a unidirectional prismatic reduction (Papagianni, 2000). The data from the unretouched blanks confirm this tendency towards laminarity (Papagianni, 2000).

Elefterochori 7

Elefterochori 7 is in Epirus, some 40 km from the coast. At least 20,000 artefacts were excavated in redeposited *terra rossa* sediments showing two layers (Fig. 1, n. 23; Ligkovanlis, 2017; Ligkovanlis et al., 2022). Artefacts belonging to Upper and Middle Palaeolithic typology were mixed (Ligkovanlis et al., 2022). The raw material is mostly flint of the Vigla formation and was imported on site preformed (Ligkovanlis, 2017). The reduction follows the discoid method, using the classic unifacial and bifacial modality, but also the Asprochaliko method on second-generation products (Ligkovanlis, 2016, 2017).

Gortses

The findspot was found during the survey conducted in 1962 by the British School of Archaeology at Athens (Fig. 1. n. 29; Dakaris et al., 1964; Papagianni, 2000). The Levallois method is attested in its lineal and recurrent centripetal modality, while the unidirectional knapping products could be either stemming from a Levallois recurrent unidirectional or a prismatic reduction (Papagianni, 2000).

The Ionian Islands

Surveys have also been carried out on the Ionian islands that are at a short distance from the coast of Epirus. Therefore, they might have been linked to the mainland during a marine lowstand or simply reached with rafts (Galanidou, 2014; Galanidou et al., 2020; Papoulia, 2017).

Lefkada and Meganisi

A survey project was conducted on the inner Ionian islands that led to the discovery of lithics scatters on the islands of Lefkada and Meganisi (Fig. 1; Galanidou, 2014, 2018; Galanidou et al., 2022). On Meganisi the lithics were found in several findspots all over the island, but also in the islet of Kythros (Galanidou, 2018; Galanidou et al., 2022). The Maganisi lithics are attributed to Levallois and discoid reductions (Galanidou et al., 2022). On Kythros, findings have been extracted mechanically from breccia sediments and are attributed to the Levallois method (Galanidou, 2018). On Lefkada, there are several collection areas: Karyotes, Cape Doukato, Englouvi, Tsoukoulades, and Marantochori. The cores are mostly flat and reduced centripetally, then attributed to the Levallois method or a surface centripetal method (Galanidou et al. 2016b). In Englouvi despite a large number of cores, the majority is globular (Galanidou et al. 2016b).

Corfu

The island of Corfu (Fig. 1) was surveyed in 1964–1966. It yielded several findspots with Middle Palaeolithic knapped stone artefacts (Papagianni, 2000; Sordinas, 1969). The analysis of the lithics produced evidence similar to that of the Epirus mainland, with abundant centripetal flaking, sometimes Levallois or attributed to the Asprochaliko method (Papagianni, 2000).

Istraishta

A lithic surface concentration was found in 2001 (Ruka et al., 2025) in the Istraishta Hills (Fig. 1, n. 2), Korça basin in southeastern Albania. The technological analysis has shown the presence of classical discoid and discoid core-on-flake reduction, and a few Levallois cores and products (Ruka et al., 2025). The discoid core-on-flake reduction, also described as Kombewa by the authors, resembles the Asprochaliko method.

Karvounari

The Karvounari area is located in the Kokkytos Valley at a short distance from the present coast of Epirus. The location was found during the survey carried out in 1962 by the

British School of Archaeology at Athens (Dakaris et al., 1964). The site consists of two main surface lithic concentrations, namely Megalo and Mikro Karvounari (Fig. 1, n. 44 and 47; Galanidou et al. 2016a; Higgs and Vita-Finzi 1966; Ligkovanlis 2011, 2017; Papagianni 2000; Papoulia 2011).

The assemblage of Megalo Karvounari from older collections consists mostly of cores and blanks with centripetal reductions and unidirectional and convergent specimens. In both cases, the Levallois method is predominant. The highest frequency of centripetal cores can be related to the final production stages (Papagianni, 2000). The new collections stem from a more recent survey project (Forsén et al., 2011, 2016). The Middle Palaeolithic artefacts from the U24 collection area show all steps of reduction. The raw material is micro-crystalline flint from the Vigla limestone formation (Ligkovanlis, 2011, 2017). The Levallois method is the most represented, with centripetal, unidirectional and preferential modalities, alongside some prismatic blade knapping (Ligkovanlis, 2011, 2017). The Levallois method is found also in other collection areas of Megalo Karvounari. Area U6 yielded bifacial tools akin to the *Keilmessergruppe* or Micoquian typologies, while one Quina scraper comes from area U7 (Galanidou et al. 2016a).

The assemblage of Mikro Karvounari from the older collections is rather small. The only two cores attest the presence of preferential Levallois modality. The unretouched blanks include also unidirectional elongated ones (Papagianni, 2000). The new collection is much larger, consisting of 978 artefacts (Papoulia, 2011). The employed technology mostly relies on Levallois, and secondarily discoid methods. The Levallois method produced centripetal flakes but also elongated unidirectional and convergent flakes (Papoulia, 2011). Some prismatic laminar flaking is present too (Papoulia, 2011).

Site PS43 was discovered in 2007. The site is located close to Mikro and Megalo Karvounari. It is a mixed assemblage of Late Upper, Upper, and Middle Palaeolithic artefacts (Fig. 1, n. 59; Galanidou & Papoulia, 2016). The 108 artefacts attributable to the Middle Palaeolithic show the use of the Levallois method (Galanidou & Papoulia, 2016).

Molondra

Molondra is located in Epirus (Fig. 1, n. 49). Excavations of colluvial *terra rossa* sediments have uncovered 1027 artefacts distributed in four layers (Ligkovanlis, 2017; Ligkovanlis et al., 2022). Artefacts typologically attributable to the Upper and Middle Palaeolithic were found mixed. However, the Middle Palaeolithic artefacts outnumber the Upper Palaeolithic ones in the lowermost layer (Ligkovanlis et al., 2022). The raw material is mostly flint of the Vigla formation. The Levallois method is the most recognisable alongside some prismatic elongated production (Ligkovanlis, 2017).

Morfi

The findspot was found in 1962 during a survey conducted by the British School of Archaeology at Athens. Recently, more surveys and test trenches have been carried out (Fig. 1, n. 50; Dakaris et al., 1964; Papagianni, 2000; Thompson et al., 2025; Tourloukis et al., 2025). The assemblage shows an admixture of Middle and Upper Palaeolithic, and possibly later, artefacts. Nevertheless, most of the findings from the newest research project have been attributed to the Middle Palaeolithic (Thompson et al., 2025). The geoarchaeological analyses of the test trenches profiles have shown the presence of a tephra deposition beneath the layer containing lithic artefacts (Tourloukis et al., 2025). The tephra has been dated to about 200 ka, providing a terminus *post quem* for the deposits lying above (Tourloukis et al., 2025). The Levallois method, in all its modalities and directions of knapping is well attested (Papagianni, 2000; Thompson et al., 2025).

Popovo

The site was found close to Elefterochori during a recent survey project (Fig. 1, n. 55; Thompson et al., 2025). It was investigated through systematic collection of artefacts on the surface, collection of artefacts from exposed profiles, and the digging of test trenches (Thompson et al., 2025; Tourloukis et al., 2025). The artefacts have been exposed to post-depositional processes that affected the preservation of the lithics, leading to the exclusion of 112 artefacts from the technological analyses. Raw material determination is still ongoing, but it is difficult due to the high degree of patination of the artefacts. In general, both tabular and nodular raw material could have been exploited (Thompson et al., 2025). Only the surface finds are sufficiently diagnostic to attribute them to the Middle Palaeolithic. The assemblage consists of cores, flakes, blades, and retouched artefacts. The technological analyses point to the use of the Levallois method, mostly in the centripetal modality. Although Levallois blades are present, there are no cores showing such a production. The retouched artefacts are typically Mousterian, mostly consisting of sidescrapers and points (Thompson et al., 2025).

The Central and southern Balkan Peninsula Middle Palaeolithic Context

The SMR1 lithic industry studied here fits well into the Middle Palaeolithic technological tradition of the Pindos area. Most of the sites involve centripetal reductions, either assigned to Levallois or discoid methods. Discerning between Levallois and discoid is not a simple endeavour, especially in small (a few hundred or fewer) and surface

scatter collections. The evidence from SMR1, one of the largest and most homogeneous assemblages so far retrieved in NW Greece, points to the use of a knapping concept involving centripetal and unidirectional products. The most interesting and comparable evidence comes from the Asprochaliko rock shelter. Here, the technological analyses showed the use of a single technological concept throughout the sequence, involving the production of centripetal flakes and pseudo-Levallois points from core-on-flakes (Ligkovanlis, 2016; Papaconstantinou, 1989). This is comparable to the *chaîne opératoire* found in SMR1. It probably implies that the SMR1 knappers selected a raw material that was adapted to their technological concept. Few radiolarite artefacts are found in SMR1, which might indicate a wider range of procurement within the Pindos (Karkanas et al., 2008; Ozsvárt et al., 2012), even though some radiolarite occur along the Mt. Vasilitsa slopes, a few kilometres away from SMR1 (Fig. 2). Looking at the broader picture available from the Balkans, the technology employed in the Middle Palaeolithic sites is coherent with that of the Pindos area (Dogandžić, 2023; Dogandžić & Đuričić, 2017; Karavanić & Banda, 2023).

Paleoenvironmental Framework of the Pindos Range Between MIS 5 and MIS 3 and Landscape Reconstruction of the Samarina Highlands

The Levallois Mousterian artefacts found in the broader study area (Biagi et al., 2022), the lithic study from SMR1, and comparisons with dated sites on both sides of the Pindos range provide evidence that the Samarina mountain landscape might have been visited by Neanderthal hunters at least as early as MIS 5e and up to early MIS 3. The paleoenvironmental characteristics of this mountain landscape at about 1500 m a.s.l. during the Upper Pleistocene can be assessed based on the regional glacial sequence of Mounts Vasilitsa and Smolikas, where catchments encompassing the studied sites are located (Biagi et al., 2022; Hughes et al., 2007; Leontaritis et al., 2020), and the nearest long lacustrine pollen sequences from Lake Ioannina (Tzedakis et al., 2002), Lake Prespa (Panagiotopoulos et al., 2013, 2014) and Lake Ochrid (Sadori et al., 2016; Sinopoli et al., 2019), which have been correlated to the MIS record and the glacial sequence of the area (Leontaritis et al., 2020). The glacial history of Mts. Smolikas and Vasilitsa indicate that glaciers formed during MIS 12 and subsequently during MIS 6, corresponding to the Skamnelian (MIS 12) and Vlasian Stage (MIS 6) within the Greek glacial chronostratigraphy, respectively. During the Vlasian Stage, glaciers covered an area of 7.8 km^2 (Hughes et al., 2007). The average equilibrium line altitude (ELA) was approximately 1997 m a.s.l. on Mt. Smolikas and 1865 m a.s.l. on Mt. Vasilitsa (Hughes et al., 2007). During the Last Glacial Cycle, the maximum extent of glaciers occurred between 30 and 25 thousand years ago; however, glaciers were present throughout the Tymphian stage (MIS 5 d to MIS 2) in the Pindos Mountains (Leontaritis et al., 2020). On Mount Smolikas, small cirque glaciers covered approximately 2.55 km^2 with a mean ELA of 2241 m a.s.l., whereas on Mount Vasilitsa, a small glacier occupied an area of 0.12 km^2 with a mean ELA of 2050 m a.s.l. (Hughes et al., 2007). Consequently, in the Samarina area, glaciers and their landforms never occurred at an altitude of 1500 m a.s.l., significant for human settlement, during the late Middle and Upper Pleistocene.

Long-term vegetation dynamics and the climate signals revealed in the pollen sequences from Lake Ioannina, Lake Prespa, and Lake Ochrid correspond accurately to the glacial and interglacial periods as well as the MIS record. The locations are situated within the mid-altitudinal zone of the southern Balkans, spanning from its lower elevations to higher altitudes (470 m a.s.l. at Lake Ioannina; 693 m a.s.l. at Lake Ohrid; 849 m a.s.l. at Lake Prespa). All three sites contain sediments that were deposited during the Upper Pleistocene. In the Lake Ioannina (Ioannina 284) pollen sequence, arboreal pollen (AP) frequency at approximately 70% characterises forested communities during the last interglacial (MIS 5e) and the interstadials of the Last Interglacial Complex (LIC) (MIS 5c and 5a). Communities with intermediate forest cover (AP between 70% and 40%) prevailed during the LIC stadials (MIS 5 d and 5b) and MIS 3. Open vegetation communities with scattered trees (AP between 40% and 21%) dominated during MIS 4 and MIS 2. *Quercus* and *Pinus* are consistently well-represented throughout the record. Additionally, during glacial intervals, several mesophilous taxa show continuous or nearly continuous pollen curves, while thermophilous taxa are characterised by intermittent presence. The data clearly indicate that temperate tree populations persisted within the region throughout the Last Glacial (Tzedakis et al., 2002).

At Lake Ohrid the long pollen sequence is characterised by dominance of non-AP (e.g. Poaceae, Chenopodiaceae and Artemisia) during glacial periods, while interglacial/interstadial periods are characterised by expansions of woodland (e.g. forests with *Abies*, *Picea*, *Quercus robur* type, *Q. cerris* type) and by increases in AP–*Pinus* pollen. More specifically, mesophilous elements such as deciduous and semi-deciduous oaks dominate forest periods of MIS 5 (Sadori et al., 2016). The Last Interglacial is characterised by wet and warm conditions, with temperatures higher than today. Subsequently, during the LIC, forested periods (interglacial and interstadials) alternated with periods of a more

open environment (stadials) (Sinopoli et al., 2019). Open vegetation formations typical of dry environments prevail during MIS 4−2 (PASZ OD-2, 70–14 ka) (Sadori et al., 2016).

Lake Prespa (core Co1215) has provided a pollen record that spans the last 92 ka BP. The base of the pollen record is characterised by high AP percentages (>70%) dominated by deciduous trees, suggesting warmer and moister conditions, which, according to the age model for the site, correspond to MIS 5. Low AP concentrations, dominance of *Pinus* and distinct *Quercus minima* characterise the pollen zones that correspond to MIS 4. Relatively high AP and a prolonged phase of moderate *Quercus* percentages correlate with MIS 3 and are interpreted as the signature of increased precipitation and higher temperatures compared to the previous MIS 4. During the Last Glacial, *Quercus* pollen is present throughout the record and potentially the Lake Prespa catchment sustained temperate tree populations throughout the period. However, AP percentage fluctuations and the intermittent appearance and very low values of some drought-sensitive taxa, such as *Fagus*, *Ulmus* and *Tilia*, indicate that during MIS 4 and MIS 2 conditions were challenging for growth at an altitude of 849 m a.s.l. (Panagiotopoulos et al., 2014).

Direct correlation of human settlement and Upper Pleistocene palaeoenvironments is available from the Middle Palaeolithic layers at Theopetra Cave. Archaeobotanical studies carried out in anthropogenic (hearths) and geogenic sediments of the cave aimed to reconstruct past vegetation under variable climatic conditions from approximately 140 to 50 thousand years (Karkanas et al., 2015; Ntinou & Kyparissi-Apostolika, 2016; Tsartsidou et al., 2015). The anthracological evidence indicates dry conditions with open park-woodland at the transition from MIS 6 to MIS 5. In continuation, a succession of temperate woodland vegetation followed by more open vegetation reflects the last interglacial and subsequent cooling (MIS 5). During the Last Glacial, cold and dry conditions are indicated by *Juniperus*-dominated vegetation, while a slight amelioration during early MIS 3 favoured open woodland expansion. Phytolith analysis of hearths and geogenic sediments demonstrated intensive human use of the cave during the last interglacial and the milder intervals of the Pleniglacial. Overall, the presence of hearths, dated by absolute methods, the material culture and archaeobotanical data indicate that Middle Palaeolithic groups would have used the site more regularly during periods of favourable climatic conditions shortly before the beginning of MIS 5, during the Last Interglacial, and the MIS 3.

The glacial record of the SMR1 study area, the three long pollen sequences in the same broader region, and the archaeological evidence allow for correlating the paleoenvironmental characteristics of the Samarina alpine landscape with human presence from MIS 5 to early MIS 3. The wet and warm conditions of the Last Interglacial would have allowed Neanderthal groups to move to highland hunting grounds after the retreat of the local glaciers of the Vlasian stage (MIS 6) and the amelioration of the climatic conditions. During the Last Glacial Cycle, although glaciers were present throughout the Tymphian stage (MIS 5d to MIS 2) in the Pindos mountains, their extent was considerably reduced compared to the penultimate glacial, and it did not reach its maximum until the Last Glacial Maximum. The long pollen sequences suggest a sensitive response of vegetation to climate change on a regional scale. Intermediate conditions in tree populations, interspersed with reductions, are observed during the stadials and interstadials of the LIC and MIS 3, while open vegetation typical of dry environments prevailed during MIS 4. After the Last Interglacial, the largest reductions in AP appear synchronous with the Heinrich events (Leontaritis et al., 2020). According to the comparison of the Lake Prespa with the Lake Ioannina record, the altitude of 849 m a.s.l. would have been roughly the upper distribution limit of drought-sensitive trees during the Late Glacial, in particular the MIS 4 (Panagiotopoulos et al., 2014). On the mountains of the study area, above this altitudinal limit and below the local glacier extent (about 2000 m a.s.l.), open patchy grasslands would have formed, rendering the Samarina mountain landscape attractive for animals and hunters alike. The area of Samarina on the Pindus, located at a crossroad between lowlands, might have been visited by groups of hunters through mountain passes, as suggested for more recent prehistoric and historic periods (Biagi et al., 2022; De Vingo et al., 2025). The absolute dates of the Middle Palaeolithic hearth layers at Theopetra Cave may provide supportive evidence for the activity of human groups in the lowlands bordering the Pindos Mountains to the east, from the end of MIS 6 to MIS 3, particularly during the last interglacial and the mild intervals of the Pleniglacial (Karkanas et al., 2015).

Conclusions

The SMR1 assemblage is a lithic collection of 1819 artefacts recovered in a cluster from a precise location and without evidence of major post-depositional disturbance. The importance of SMR1 stems from its high-altitude location, showing for the first time in the southern Balkans the exploitation of mountain environment by groups of Neanderthals in their seasonal movements. Despite the fact that the presence of Neanderthals in the mountains was a behaviour known since long (Radmilli, 1965), the Greek mountains had never been investigated before searching for Palaeolithic sites.

The assemblage has been collected avoiding bias, ensuring that also the smallest and indeterminable fragments are available. Additionally, no artefact can be attributed either to the Upper Palaeolithic or later periods, and no ceramic potsherds have been noticed. These observations suggest the pristine condition of the lithic concentration and contribute to underline the importance of SMR1 for the reconstruction of the Middle Palaeolithic occupation of the south Balkan Peninsula in general, and the Pindos Mountains range in particular, an area previously mostly devoid of research. The techno-typological study of the lithic assemblage revealed a coherent technological pattern showing the presence of a single *chaîne opératoire* starting from the raw material procurement and the reduction on-site through centripetal surface knapping. This technological behaviour is comparable to most of the southern Balkan Peninsula Middle Palaeolithic sites and findspots. However, the most striking similarity might be drawn with the Asprochaliko rock shelter assemblage and the use of centripetal knapping on ventral flake surfaces (Ligkovanlis, 2016; Papaconstantinou, 1989).

According to the lithic evidence and comparison with dated sites, SMR1 might be attributed to the Upper Pleistocene (MIS 5 to early MIS 3). The evidence from the other lithic findspots documented in the Samariniotikos Valley and the surrounding mountain ridges (Biagi et al., 2017, Fig. 6) suggest that SMR1 represents a location for lithic production activities of Neanderthal groups exploiting the whole landscape, maybe in seasonal visits.

New research should be devoted to improving the geoarchaeological interpretation of the landscape evolution and of the SMR1 site, especially assessing the soil dynamics of the profile from which the lithics are eroding.

Supplementary Information The online version contains supplementary material available at https://doi.org/10.1007/s41982-026-00260-7.

Acknowledgements The authors are very grateful to the Ephorate of Prehistoric and Classical Antiquities (L'EPKA) of Kozani, Ephorate of Antiquities (EFA) of Grevena, and the Greek Ministry of Culture for granting the research permit and for their support. Thanks for support during fieldwork are due to Dr Renato Nisbet and Prof. Diego E. Angelucci. This paper is dedicated to Nikos Efstratiou, the leader of the Samarina Archaeological Project who is no longer with us. The team that has worked with him through the years acknowledges his pioneering ideas, scientific dedication and unconditional support. He will be remembered with affection and gratitude.

Author contributions Conceptualization: P.B., J.G., M.N., E.S.; Methodology: J.G.; Formal analysis and investigation: J.G.; Writing - original draft preparation: P.B., N.E., J.G., M.N., E.S.; Funding acquisition: P.B., N.E., J.G., E.S.; Resources: N.E. All authors reviewed the manuscript.

Funding Open access funding provided by Università degli Studi di Cagliari within the CRUI-CARE Agreement. The research in the Pindos Mountains of Western Macedonia was made possible thanks to the financial support of the Municipality of Grevena, the Prefecture of Western Macedonia, the Institute of Aegean Prehistory (INSTAP, USA), the ADiR (Assegnazione Dipartimentale per la Ricerca) Department of Asian and North African Studies of the University Ca' Foscari, Venice, the Aristotle University, Thessaloniki (Greece), Departmental Project Funds of Ca' Foscari University, Venice. E.S. was supported by the University of Pisa (Italy) and the Excellence Project of the Department of Civilizations and Forms of Knowledge (n. 429999-DIP ECCELL-CIVILTA-2018-2022) awarded by the Italian Ministry of University and Research (MUR). J.G. was founded in the framework of the Horizon Europe funding programme Marie Sklodowska Curie Actions Postdoctoral Fellowship scheme (MobiliTy – nr. 101061427) awarded by the European Commission, and he is currently supported by the NEANDURANCE project (I53C25000840006) funded by the NextGenerationEU – Young Researchers 2024 funding scheme awarded by the Italian Ministry of University and Research (MUR). Article Processing Charge costs are provided to the Corresponding Author (ES) by University of Cagliari, under the agreement CARE-CRUI.

Data Availability The Authors declare that all the data underlying the manuscript are available in the manuscript itself or within the Supporting Information files.

Declarations

Competing interests The authors declare no competing interests.

References

Alex, B., Mihailović, D., Milošević, S., & Boaretto, E. (2019). Radiocarbon chronology of Middle and Upper Paleolithic sites in Serbia, Central Balkans. *Journal of Archaeological Science: Reports*, *25*, 266–279. https://doi.org/10.1016/j.jasrep.2019.04.010

Ammerman, A. J., Efstratiou, N., & Adam, E. (1999). First Evidence for the Palaeolithic in Aegean Thrace. In The palaeolithic archaeology of Greece and adjacent areas: proceedings of the ICOPAG conference, Ioannina, September 1994 (Vol. 3, pp. 211–214). British School at Athens Studies.

Badino, F., Ruka, R., Pini, R., Frechen, M., Argante, V., Susini, D., et al. (2025). Palaeoenvironmental, stratigraphic and geochronological study of the coastal site of Dalani i Vogël (Vlora, Albania): New evidence for late Neanderthal occupation and prehistoric archaeology. *Quaternary Science Reviews, 349*, Article 109111. https://doi.org/10.1016/j.quascirev.2024.109111

Bailey, G. N., Papaconstantinou, E., & Sturdy, D. (1992). Asprochaliko and Kokkinopilos: TL Dating and reinterpretation of Middle Palaeolithic sites in Epirus, North-West Greece. *Cambridge Archaeological Journal, 2*(1), 136–144.

Biagi, P., Nisbet, R., Michniak, R., & Efstratiou, N. (2015). The chert outcrops of the Pindus Range of Western Macedonia (Greece)

and their middle palaeolithic exploitation. *The Quarry - The e-Newsletter of the SAA's Prehistoric Quarries & Early Mines Interest Group, 11*, 3–16.

Biagi, P., Nisbet, R., Starnini, E., Efstratiou, N., & Michniak, R. (2017). Where mountains and Neanderthals meet: The Middle Palaeolithic settlement of Samarina in the Northern Pindus (Western Macedonia, Greece). *Eurasian Prehistory*, *13*(1), 3–76.

Biagi, P., Starnini, E., Efstratiou, N., Nisbet, R., Hughes, P. D., & Woodward, J. C. (2022). Mountain landscape and human settlement in the Pindus Range: The Samarina Highland Zones of Western Macedonia, Greece. *Land, 12*(1), Article 96. https://doi.org/10.3390/land12010096

Boëda, É. (1993). Le débitage discoïde et le débitage Levallois récurrent centripède. *Bulletin de la Société Préhistorique Française, 90*(6), 392–404. https://doi.org/10.3406/bspf.1993.9669

Boëda, É. (1994). *Le concept Levallois: Variabilité des méthodes*. CNRS Édition.

Bona, F., Peresani, M., & Tintori, A. (2007). Indices de fréquentation humaine dans les grottes à ours au Paléolithique moyen final. *L'Anthropologie, 111*(3), 290–320. https://doi.org/10.1016/j.anthro.2007.05.003

Bordes, F. (1961). *Typologie du Paléolithique ancien et moyen*. Delmas.

Bordes, F. (1988). *Typologie du Paléolithique ancien et moyen*. CNRS Édition.

Bustos-Pérez, G., Baena, J., & Vaquero, M. (2023). What lies in between: Levallois, discoid and intermediate methods. *Journal of Lithic Studies*, *10*(2), 32p–332. https://doi.org/10.2218/jls.7132

Carmignani, L., & Soressi, M. (2023). Ahead of the times: Blade and bladelet production associated with Neandertal remains at the Bau de l'Aubesier (Mediterranean France) between MIS 7 and MIS 5d. *PaleoAnthropology, 2023*(1), 1–33. https://doi.org/10.48738/2023.iss1.127

Dakaris, S. I., Higgs, E. S., & Hey, R. W. (1964). The Climate, Environment and Industries of Stone Age Greece: Part I. *Proceedings of the Prehistoric Society, 30*, 199–244. https://doi.org/10.1017/S0079497X00015139

Darlas, A. (2007). Le Moustérien de Grèce à la lumière des récentes recherches. *L'Anthropologie, 111*(3), 346–366. https://doi.org/10.1016/j.anthro.2007.04.001

Delpiano, D., Gennai, J., & Peresani, M. (2021). Techno-functional implication on the production of discoid and Levallois backed implements. *Lithic Technology*. https://doi.org/10.1080/01977261.2021.1886487

De Vingo, P., Merlini, V., Biagi, P., Starnini, E., & Efstratiou, N. (2025). Pottery as an indicator of mountain landscape exploitation: An example from the Northern Pindos Range of Western Macedonia (Greece). *Heritage, 8*(12), Article 500. https://doi.org/10.3390/heritage8120500

Dogandžić, T. (2023). The Middle Paleolithic of the Balkans: Industrial variability, human biogeography, and Neanderthal demise. *Journal of World Prehistory, 36*(2), 257–338. https://doi.org/10.1007/s10963-023-09179-1

Dogandžić, T., & Đuričić, L. (2017). Lithic production strategies in the Middle Paleolithic of the southern Balkans. *Quaternary International*, *450*, 68–102. https://doi.org/10.1016/j.quaint.2017.03.011

Domingo, R., Peña-Monné, J. L., De Torres, T., Ortiz, J. E., & Utrilla, P. (2017). Neanderthal highlanders: Las Callejuelas (Monteagudo del Castillo, Teruel, Spain), a high-altitude site occupied during MIS 5. *Quaternary International, 435*, 129–143. https://doi.org/10.1016/j.quaint.2015.09.088

Doronicheva, E. V., Golovanova, L. V., Doronichev, V. B., Tregub, T. F., Tselmovitch, V. A., & Korzinova, A. S. (2024). Hominin Occupation of the North-Central Caucasus During the Middle Paleolithic: New Results from Saradj-Chuko Grotto and the State of Research. *PaleoAnthropology*, 63–86. https://doi.org/10.48738/2024.ISS1.1134

Efstratiou, N., Biagi, P., Angelucci, D. E., & Nisbet, R. (2011). Middle Palaeolithic chert exploitation in the Pindus Mountains of western Macedonia, Greece. *Antiquity Project Gallery*, 85(328).

Efstratiou, N., Biagi, P., Elefanti, P., Karkanas, P., & Ntinou, M. (2006). Prehistoric exploitation of Grevena highland zones: Hunters and herders along the Pindus chain of western Macedonia (Greece). *World Archaeology, 38*(3), 415–435. https://doi.org/10.1080/00438240600813327

Elefanti, P., & Marshall, G. (2015). Late Pleistocene hominin adaptations in Greece. In F. Coward, R. Hosfield, M. Pope, & F. Wenban-Smith (Eds.), Settlement, Society and Cognition in Human Evolution (1st ed., pp. 189–213). Cambridge University Press. https://doi.org/10.1017/CBO9781139208697.012

Facorellis, Y., Karkanas, P., Higham, T., Brock, F., Ntinou, M., & Kyparissi-Apostolika, N. (2013). Interpreting radiocarbon dates from the Paleolithic layers of Theopetra Cave in Thessaly, Greece. *Radiocarbon, 55*(3), 1432–1442. https://doi.org/10.1017/S0033822200048360

Falguères, C., Shao, Q., Perrenoud, C., Stringer, C., Tombret, O., Garbé, L., & Darlas, A. (2025). New U-series dates on the Petralona cranium, a key fossil in European human evolution. *Journal of Human Evolution, 206*, Article 103732. https://doi.org/10.1016/j.jhevol.2025.103732

Forestier, H. (1993). Le Clactonien: Mise en application d'une nouvelle méthode de débitage s'inscrivant dans la variabilité des systèmes de production lithique du Paléolithique ancien. *Paléo*, *5*(1), 53–82. https://doi.org/10.3406/pal.1993.1104

Forsén, B., Galanidou, N., & Tikkala, E. (2016). *Thesprotia expedition*. Suomen Ateenan-Instituutin säätiö.

Forsén, B., & Tikkala, E. (2011). *Thesprotia expedition II: Environment and settlement patterns*. Suomen Ateenan-Instituutin säätiö.

Francis, K., Gilkes, O., Gjtipali, I., Polci, B., Powell, A., Skeates, R., & Vulpi, V. (2005). Explorations in Albania, 1930-39: The notebooks of Luigi Cardini, prehistoria with the Italian archaeological mission. *The British School at Athens Supplementary Volumes*, *37*, 1–222.

Galanidou, N. (2014). Inner Ionian Sea Archipelago: Archaeological Survey. In C. Smith (Ed.), *Encyclopedia of Global Archaeology* (pp. 3882–3888). Springer New York. https://doi.org/10.1007/978-1-4419-0465-2_1314

Galanidou, N. (2018). Parting the waters. Middle Palaeolithic archaeology in the central Ionian Sea. *Journal of Greek Archaeology, 3*, 1–22.

Galanidou, N., Dellaporta, K., & Sakellariou, D. (2020). Greece: Unstable Landscapes and Underwater Archaeology. In G. N. Bailey, N. Galanidou, H. Peeters, H. Jöns, & M. Mennenga (Eds.), *The Archaeology of Europe's Drowned Landscapes* (Vol. 35, pp. 371–392). Springer International Publishing. https://doi.org/10.1007/978-3-030-37367-2_19

Galanidou, N., Gatsi, M., Vikatou, O., Vasilakis, A., Morgan, C., & Forsén, J. (2022). Prehistoric settlement in the Inner Ionian Sea Archipelago and its Ionian island connections. In C. Souyoudzoglou-Haywood & C. Papoulia (Eds.), Archaeology of the Ionian Sea: Landscapes, seascapes and the circulation of people, goods and ideas from the Palaeolithic to end of the Bronze Age (pp. 29–40). Oxbow Books. https://doi.org/10.2307/j.ctv22fqc0s

Galanidou, N., Iliopoulos, G., & Papoulia, C. (2016b). The Palaeolithic settlement of Lefkas. Archaeological evidence in a palaeogeographic context. *Journal of Greek Archaeology, 1*, 1–33. https://doi.org/10.32028/jga.v1i.642

Galanidou, N., & Papoulia, C. (2016). PS 43: A Multi-period Stone Age Site on the Kokytos Valley Bottom. In B. Forsén, N. Galanidou, & E. Tikkala (Eds.), *Thesprotia expedition. III: Landscapes*

of nomadism and sedentism (pp. 99–120). Suomen Ateenan-Instituutin säätiö.

Galanidou, N., Papoulia, C., & Ligkovanlis, S. (2016a). The Middle Palaeolithic Bifacial Tools from Megalo Karvounari. In B. Forsén, N. Galanidou, & E. Tikkala (Eds.), *Thesprotia expedition. III: Landscapes of nomadism and sedentism* (pp. 29–58). Suomen Ateenan-Instituutin säätiö.

Garefalakis, C., Panagopoulou, E., & Harvati, K. (2018). Late Pleistocene Neanderthal occupation of Western Mani: The evidence from the Middle Palaeolithic assemblages of Mavri Spilia. *Quaternary International*, *497*, 4–13. https://doi.org/10.1016/j.quaint.2017.12.049

Gasparyan, B., Egeland, C., Adler, D. S., Pinhasi, R., Glauberman, P., & Haydosyan, H. (2014). The Middle Paleolithic Occupation of Armenia: Summarizing Old and New Data. In B. Gasparyan & M. Arimura (Eds.), *Stone age of Armenia: A guide-book to the stone age archaeology in the Republic of Armenia* (pp. 65–105). Center for Cultural Resource Studies.

GEBCO Bathymetric Compilation Group (2023). (2023). The GEBCO_2023 Grid - a continuous terrain model of the global oceans and land. NERC EDS British Oceanographic Data Centre NOC. https://doi.org/10.5285/F98B053B-0CBC-6C23-E053-6C86ABC0AF7B

González-Molina, I., Jiménez-García, B., Maíllo-Fernández, J.-M., Baquedano, E., & Domínguez-Rodrigo, M. (2020). Distinguishing Discoid and Centripetal Levallois methods through machine learning. *PLoS One, 15*(12), Article e0244288. https://doi.org/10.1371/journal.pone.0244288

Guette, C. (2002). Révision critique du concept de débitage Levallois à travers l'étude du gisement moustérien de Saint-Vaast-la-Hougue/le Fort (chantiers I-III et II, niveaux inférieurs) (Manche, France). *Bulletin de la Société Préhistorique Française, 99*(2), 237–248. https://doi.org/10.3406/bspf.2002.12655

Harrold, F. B., Korkuti, M. M., Ellwood, B. B., Petruso, K. M., & Schuldenrein, J. (1999). The Palaeolithic of Southernmost Albania. In The palaeolithic archaeology of Greece and adjacent areas: proceedings of the ICOPAG conference, Ioannina, September 1994 (Vol. 3, pp. 361–372). British School at Athens Studies.

Harvati, K., Panagopoulou, E., Karkanas, P., Athanassiou, A., & Frost, S. R. (2008). Preliminary results of the Aliakmon palaeolithic/palaeoanthropological survey, Greece, 2004–2005. In A. Darlas & D. Mihailović (Eds.), *The Palaeolithic of the Balkans* (pp. 15–20). Archaeopress.

Harvati, K., Röding, C., Bosman, A. M., Karakostis, F. A., Grün, R., Stringer, C., et al. (2019). Apidima Cave fossils provide earliest evidence of *Homo sapiens* in Eurasia. *Nature, 571*(7766), 500–504. https://doi.org/10.1038/s41586-019-1376-z

Harvati, K., & Roksandic, M. (Eds.). (2016). *Paleoanthropology of the Balkans and Anatolia: Human Evolution and its Context*. Springer Netherlands. https://doi.org/10.1007/978-94-024-0874-4

Hauck, T. C., Ruka, R., Gjipali, I., Richter, J., & Nolde, N. (2017). The "German Albanian Palaeolithic" Programme (GAP): A status report. In M. Otte (Ed.), *Vocation préhistoire: Hommage à Jean-Marie Le Tensorer* (Vol. 1–148, pp. 159–173). ERAUL.

Hershkovitz, I., Weber, G. W., Quam, R., Duval, M., Grün, R., Kinsley, L., et al. (2018). The earliest modern humans outside Africa. *Science, 359*(6374), 456–459. https://doi.org/10.1126/science.aap8369

Higgs, E. S., & Vita-Finzi, C. (1966). The climate, environment and industries of Stone Age Greece: Part II. *Proceedings of the Prehistoric Society, 32*, 1–29. https://doi.org/10.1017/S0079497X00014328

Hughes, P. D., Gibbard, P. L., & Woodward, J. C. (2007). Geological controls on Pleistocene glaciation and cirque form in Greece. *Geomorphology, 88*(3–4), 242–253. https://doi.org/10.1016/j.geomorph.2006.11.008

Inizan, M. L., Reduron-Ballinger, M., Roche, H., & Tixier, J. (1999). *Technology and terminology of knapped stone: followed by a multilingual vocabulary*. CREP. - Arabic, English, French, German, Greek, Italian, Portuguese, Spanish. (J. Féblot-Augustins, Trans.).

Jéquier, J. P. (1975). *Le Moustérien alpin: révision critique. Eburodunum 2, Cahiers d'archéologie romande de la Bibliothèque historique vaudoise, 2*. Institut d'archéologie yverdonnoise.

Karavanić, I., & Banda, M. (2023). The Middle Palaeolithic of South-eastern Europe. In A. Ruiz-Redondo & W. Davies (Eds.), *The Prehistoric hunter-gatherers of South-Eastern Europe* (pp. 60–106). Oxford University Press.

Karkanas, P. (1999). Lithostratigraphy and micromorphology of Theopetra Cave deposits, Thessaly, Greece: Some preliminary results. In G. N. Bailey (Ed.), *The palaeolithic archaeology of Greece and adjacent areas: Proceedings of the ICOPAG conference, Ioannina, September 1994* (pp. 240–251). British School at Athens.

Karkanas, P., & Kyparissi-Apostolika, N. (2024). Revisiting palaeolithic combustion features of Theopetra Cave: A diachronic use of dung and peat as fuel. *Journal of Archaeological Science, 165*, Article 105958. https://doi.org/10.1016/j.jas.2024.105958

Karkanas, P., Panagopoulou, E., Anoussis, J., & Kyparissi-Apostolika, N. (2008). Raw material procurement in the Middle Palaeolithic of Thessaly: sourcing studies. In Proceedings of the 4th symposium of the Hellenic Society for Archaeometry: National Hellenic Research Foundation, Athens, 28–31 may 2003. Oxford: Archaeopress.

Karkanas, P., White, D., Lane, C. S., Stringer, C., Davies, W., Cullen, V. L., et al. (2015). Tephra correlations and climatic events between the MIS6/5 transition and the beginning of MIS3 in Theopetra Cave, central Greece. *Quaternary Science Reviews, 118*, 170–181. https://doi.org/10.1016/j.quascirev.2014.05.027

Kyparissi-Apostolika, N. (1999). The Palaeolithic deposits of Theopetra Cave in Thessaly (Greece). In G. N. Bailey (Ed.), *The palaeolithic archaeology of Greece and adjacent areas: Proceedings of the ICOPAG conference, Ioannina, September 1994* (pp. 232–239). British School at Athens.

Kyparissi-Apostolika, N., & Manolis, K. S. (2021). Reconsideration of the Antiquity of the Middle Palaeolithic Footprints from Theopetra Cave (Thessaly, Greece). In A. Pastoors & T. Lenssen-Erz (Eds.), *Reading Prehistoric Human Tracks: Methods & Material* (pp. 169–182). Springer International Publishing. https://doi.org/10.1007/978-3-030-60406-6

Laplace, G. (1964). Essai de Typologie Systématique. *Annali dell'Università di Ferrara, I*(Supplemento II), 3–85.

Leontaritis, A. D., Kouli, K., & Pavlopoulos, K. (2020). The glacial history of Greece: A comprehensive review. *Mediterranean Geoscience Reviews, 2*(1), 65–90. https://doi.org/10.1007/s42990-020-00021-w

Ligkovanlis, S. (2011). Megalo Karvounari Revisited. In B. Forsén & E. Tikkala (Eds.), *Thesprotia expedition II: Environment and settlement patterns* (pp. 159–180). Suomen Ateenan-Instituutin säätiö.

Ligkovanlis, S. (2016). On lithic technology terms and semantics. The example of the Asprochaliko Rockshelter Middle Palaeolithic stone industry. In P. Elefanti, P. N. Kardulias, & G. Marshall (Eds.), *Lithics past and present: Perspectives on chipped stone studies in Greece* (Vol. CXLIV, pp. 95–109). Åströms förlag.

Ligkovanlis, S. (2017). New insights into the Upper Pleistocene archaeology of Northwestern Greece: The evidence from three open-air sites and its implication for Middle and Upper Palaeolithic hunter-gatherers' activity and behaviour in Southeastern Europe. *Journal of Greek Archaeology*, *2*, 1–32. https://doi.org/10.32028/jga.v2i.569

Ligkovanlis, S., Iliopoulos, G., Palli, O., Tzortzatou, A., & Tsakanikou, P. (2022). Palaeolithic artifact taphonomy in terra rossa sites

at Northwestern Greece revisited: Two new case studies. *Mediterranean Archaeology and Archaeometry, 22*(3), 215–229. https://doi.org/10.5281/ZENODO.7306045

Ligkovanlis, S., & Kourtessi-Philippakis, G. (2022). Palaeolithic chipped stone industries from Zakynthos, Ionian islands, Greece. Interpreting the new evidence within the western Greek and Adriatic context. In Archaeology of the Ionian Sea: Landscapes, seascapes and the circulation of people, goods and ideas from the Palaeolithic to end of the Bronze Age (pp. 41–52).

Malinsky-Buller, A., Glauberman, P., Ollivier, V., Lauer, T., Timms, R., Frahm, E., et al. (2021). Short-term occupations at high elevation during the Middle Paleolithic at Kalavan 2 (Republic of Armenia). *PLoS One, 16*(2), Article e0245700. https://doi.org/10.1371/journal.pone.0245700

Margaritora, D., Dozio, A., Chelidonio, G., Turrini, M. C., & Peresani, M. (2020). The Lower and Middle Palaeolithic settlements in the Baldo-Lessini mountains. Results from a GIS investigation. *Alpine and Mediterranean Quaternary*, *33*(1), 115–132. https://doi.org/10.26382/AMQ.2020.13

Mihailović, D. (2008). New data about the Middle Palaeolithic of Serbia. In A. Darlas & D. Mihailović (Eds.), *The Palaeolithic of the Balkans.* Archaeopress.

Mihailović, D. (2014). *Palaeolithic and Mesolithic research in the Central Balkans*. Serbian Archeological Society.

Mihailović, D. (2020). Push-and-pull factors of the Middle to Upper Paleolithic transition in the Balkans. *Quaternary International*, *551*, 47–62. https://doi.org/10.1016/j.quaint.2019.10.010

Mihailović, D., Kuhn, S. L., Bogićević, K., Dimitrijević, V., Marín-Arroyo, A. B., Marković, J., et al. (2022). Connections between the Levant and the Balkans in the late Middle Pleistocene: Archaeological findings from Velika and Mala Balanica Caves (Serbia). *Journal of Human Evolution, 163*, Article 103138. https://doi.org/10.1016/j.jhevol.2021.103138

Mihailović, D., & Whallon, R. (2017). Crvena Stijena revisited: The Late Mousterian assemblages. *Quaternary International*, *450*, 36–49. https://doi.org/10.1016/j.quaint.2016.12.026

Monnier, G., Tostevin, G. B., Pajović, G., Borovonić, N., & Baković, M. (2020). Nova istraživanja paleolitskog nalazišta Crvena Stijena, istorijski kontekst/New Research at the Paleolithic Site of Crvena Stijena, Nikšic Municipality, Montenegro Within Its Historical Context. *Istorijski Zapisi, XCIII*, 71–108.

Ntinou, M., & Kyparissi-Apostolika, N. (2016). Local vegetation dynamics and human habitation from the last interglacial to the early Holocene at Theopetra cave, central Greece: The evidence from wood charcoal analysis. *Vegetation History and Archaeobotany, 25*(2), 191–206. https://doi.org/10.1007/s00334-015-0538-7

Ozsvárt, P., Dosztály, L., Migiros, G., Tselepidis, V., & Kovács, S. (2012). New radiolarian biostratigraphic age constraints on Middle Triassic basalts and radiolarites from the Inner Hellenides (Northern Pindos and Othris Mountains, Northern Greece) and their implications for the geodynamic evolution of the early Mesozoic Neotethys. *International Journal of Earth Sciences, 101*(6), 1487–1501. https://doi.org/10.1007/s00531-010-0628-9

Panagiotopoulos, K., Aufgebauer, A., Schäbitz, F., & Wagner, B. (2013). Vegetation and climate history of the Lake Prespa region since the lateglacial. *Quaternary International, 293*, 157–169. https://doi.org/10.1016/j.quaint.2012.05.048

Panagiotopoulos, K., Böhm, A., Leng, M. J., Wagner, B., & Schäbitz, F. (2014). Climate variability over the last 92 ka in SW Balkans from analysis of sediments from Lake Prespa. *Climate of the Past*, *10*(2), 643–660. https://doi.org/10.5194/cp-10-643-2014

Panagopoulou, E. (1999). The Theopetra Middle Palaeolithic assemblages: Their relevance to the Middle Palaeolithic of Greece and adjacent areas. In G. N. Bailey (Ed.), *The palaeolithic archaeology of Greece and adjacent areas: Proceedings of the ICOPAG conference, Ioannina, September 1994* (pp. 252–265). British School at Athens.

Papaconstantinou, E. (1989). Micromoustérien: les idées e les pierres. Asprochaliko (Grèce) et le problème des industries microlithiques du Moustérien (Doctoral thesis). Université de Paris X Nanterre, Paris.

Papagianni, D. (1999). Beyond 'flint scatters' and 'findspots': Assessing the potential for compiling a synthesis of the Greek Middle Palaeolithic surface data. In G. N. Bailey (Ed.), *The palaeolithic archaeology of Greece and adjacent areas: Proceedings of the ICOPAG conference, Ioannina, September 1994* (pp. 130–136). British School at Athens.

Papagianni, D. (2000). *Middle Palaeolithic Occupation and Technology in Northwestern Greece*. BAR Publishing. https://doi.org/10.30861/9781841711492

Papoulia, C. (2011). Mikro Karvounari in context: The new lithic collection and its implications for Middle Palaeolithic hunting activities. In B. Forsén & E. Tikkala (Eds.), *Thesprotia expedition II: Environment and settlement patterns* (pp. 123–158). Suomen Ateenan-Instituutin säätiö.

Papoulia, C. (2017). Seaward dispersals to the NE Mediterranean islands in the Pleistocene. The lithic evidence in retrospect. *Quaternary International*, *431*, 64–87.

Patil, I. (2021). Visualizations with statistical details: The "ggstatsplot" approach. *Journal of Open Source Software, 6*(61), Article 3167. https://doi.org/10.21105/joss.03167

Peresani, M. (2003). *Discoid lithic technology: Advances and implications*. Archaeopress.

Peresani, M. (2012). Fifty thousand years of flint knapping and tool shaping across the Mousterian and Uluzzian sequence of Fumane cave. *Quaternary International*, *247*, 125–150. https://doi.org/10.1016/j.quaint.2011.02.006

Posth, C., Wißing, C., Kitagawa, K., Pagani, L., Van Holstein, L., Racimo, F., et al. (2017). Deeply divergent archaic mitochondrial genome provides lower time boundary for African gene flow into Neanderthals. *Nature Communications, 8*(1), Article 16046. https://doi.org/10.1038/ncomms16046

Radmilli, A. M. (1965). *Abruzzo preistorico: Il paleolitico inferiore-medio abruzzese*. Sansoni.

R Core Team (2025). _R: A Language and Environment for Statistical Computing_. R Foundation for Statistical Computing. Vienna. Austria. https://www.R-project.org/

Ruka, R. (2023). The Lithic Assemblages. In M. L. Galaty & L. Bejko (Eds.), *Archa eological investigations in a Northern Albanian Province: results of the Projetki Arkeologjik i Shkodres (PASH)/ Volume 2: Artifacts and Artifact Analysis* (pp. 2–43). Ann Arbor, Michigan: University of Michigan.

Ruka, R., Bassetti, M., Bertola, S., Delpiano, D., Gjipali, I., & Peresani, M. (2025). Middle Palaeolithic in Southern Albania: Perspectives from the lithic industry of the Istraishta site. *Alpine and Mediterranean Quaternary, 38*(1), 1–26. https://doi.org/10.26382/AMQ.2025.01

Ruka, R., Gjipali, I., Galaty, M. L., & Bajramaj, N. (2014). Lithics at one end of the circum-Adriatic: case studies from the southernmost Albanian coastal lowland. In L. Përzhita, I. Gjipali, G. Hoxha, & B. Muka (Eds.), Proceedings of the International Congress of Albanian Archaeological Studies: 65th anniversary of Albanian archaeology (21–22 November, Tirana 2013) (pp. 93–106). Tiranë: Botimet Albanologjike. https://doi.org/10.13140/2.1.4530.0807. Accessed 23 November 2023.

Runnels, C. N. (1988). A prehistoric survey of Thessaly: New Light on the Greek Middle Paleolithic. *Journal of Field Archaeology, 15*(3), 277–290.

Runnels, C. N., Korkuti, M., Galaty, M. L., Timpson, M. E., Stocker, S. R., Davis, J. L., et al. (2010). Early prehistoric landscape and landuse in the Fier Region of Albania. *Journal of Mediterranean*

Archaeology, 22(2), 151–182. https://doi.org/10.1558/jmea.v22i2.151

Runnels, C. N., Korkuti, M., Galaty, M. L., Timpson, M. E., Whittaker, J. C., Stocker, S. R., et al. (2004). The Palaeolithic and Mesolithic of Albania: Survey and Excavation at the Site of Kryegjata B (Fier District). *Journal of Mediterranean Archaeology*, *17*(1), 3–30. https://doi.org/10.1558/jmea.17.1.3.53480

Runnels, C. N., & Van Andel, T. H. (2003). The Early Stone Age of the Nomos of Preveza: Landscape and Settlement. In J. Wiseman & K. Zachos (Eds.), Landscape Archaeology in Southern Epirus (Vol. 32, pp. 47–134). The American School of Classical Studies at Athens. https://www.jstor.org/stable/1354046?origin=crossref. Accessed 14 November 2023.

Sadori, L., Koutsodendris, A., Panagiotopoulos, K., Masi, A., Bertini, A., Combourieu-Nebout, N., et al. (2016). Pollen-based paleoenvironmental and paleoclimatic change at Lake Ohrid (southeastern Europe) during the past 500 ka. *Biogeosciences, 13*(5), 1423–1437. https://doi.org/10.5194/bg-13-1423-2016

Sinopoli, G., Peyron, O., Masi, A., Holtvoeth, J., Francke, A., Wagner, B., & Sadori, L. (2019). Pollen-based temperature and precipitation changes in the Ohrid Basin (western Balkans) between 160 and 70 ka. *Climate of the Past, 15*(1), 53–71. https://doi.org/10.5194/cp-15-53-2019

Sordinas, A. (1969). Investigations of the prehistory of Corfu during 1964–1966. *Balkan Studies, 10*, 394–424.

Soressi, M., & Geneste, J.-M. (2011). The history and efficacy of the Chaîne Opératoire approach to lithic analysis: Studying techniques to reveal past societies in an evolutionary perspective. *PaleoAnthropology, Special Issue: Reduction Sequence, Chaîne Opératoire, and Other Methods: The Epistemologies of Different Approaches to Lithic Analysis*, 334–350.

Spathas, S. A. (2023). Agia: An open-air Middle Paleolithic site in Northwestern Greece. *Journal of Balkan Studies, 3*(1), 45–58. https://doi.org/10.51331/A036

Stojanovski, D., Berruti, G. L. F., Arzarello, M., Lacy, S. A., Nacev, T., & Danev, A. (2025). Technology and taphonomy of the Middle Paleolithic assemblage from the Uzun Mera site in Macedonia. *Quaternary Environments and Humans, 3*(2), Article 100069. https://doi.org/10.1016/j.qeh.2025.100069

Thompson, N., Kourtessi-Philippakis, G., Giusti, D., Harvati, K., & Tourloukis, V. (2025). The preliminary study of lithic assemblages from the archaeological survey and test trench excavations at Popovo and Morfi, Greece. In K. Harvati & M. Ioannidou (Eds.), Human Evolution at the CROSSROADS: Research in Greece and beyond. Proceedings of the Closing Symposium, February 2022 (Vol. 3, pp. 269–280). Tübingen University Press. https://publikationen.uni-tuebingen.de/xmlui/handle/10900/156256. Accessed 15 September 2025.

Tillet, T. (2003). Il Paleolitico medio e inferiori nelle Alpi e dintorni. *Preistoria Alpina*, *39*, 49–58.

Tourloukis, E. (2010). *The early and middle Pleistocene archaeological record of Greece: Current status and future prospects*. Leiden University Press.

Tourloukis, E., & Harvati, K. (2018). The palaeolithic record of Greece: A synthesis of the evidence and a research agenda for the future. *Quaternary International, 466*, 48–65. https://doi.org/10.1016/j.quaint.2017.04.020

Tourloukis, E., Karkanas, P., & Wallinga, J. (2015). Revisiting Kokkinopilos: Middle Pleistocene radiometric dates for stratified archaeological remains in Greece. *Journal of Archaeological Science*, *57*, 355–369. https://doi.org/10.1016/j.jas.2015.03.012

Tourloukis, E., Kourtessi-Philippakis, G., Karkanas, P., Nomade, S., Giusti, D., & Thompson, N. (2025). Geoarchaeological and geochronological investigations of Palaeolithic open-air sites in Epirus, Greece. In K. Harvati & M. Ioannidou (Eds.), Human Evolution at the CROSSROADS: Research in Greece and beyond. Proceedings of the Closing Symposium, February 2022 (Vols 1–3, pp. 259–267). Universität Tübingen. Accessed 15 September 2025. https://publikationen.uni-tuebingen.de/xmlui/handle/10900/156257

Tourloukis, E., Thompson, N., Garefalakis, C., Karkanas, P., Konidaris, G. E., Panagopoulou, E., & Harvati, K. (2016). New Middle Palaeolithic sites from the Mani Peninsula, Southern Greece. *Journal of Field Archaeology, 41*(1), 68–83. https://doi.org/10.1080/00934690.2015.1125223

Tsartsidou, G., Karkanas, P., Marshall, G., & Kyparissi-Apostolika, N. (2015). Palaeoenvironmental reconstruction and flora exploitation at the palaeolithic cave of Theopetra, central Greece: The evidence from phytolith analysis. *Archaeological and Anthropological Sciences, 7*(2), 169–185. https://doi.org/10.1007/s12520-014-0183-6

Tzedakis, P. C., Lawson, I. T., Frogley, M. R., Hewitt, G. M., & Preece, R. C. (2002). Buffered tree population changes in a Quaternary Refugium: Evolutionary implications. *Science, 297*(5589), 2044–2047. https://doi.org/10.1126/science.1073083

Valladas, H., Mercier, N., Froget, L., Joron, J.-L., Reyss, J.-L., Karkanas, P., et al. (2007). TL age-estimates for the Middle Palaeolithic layers at Theopetra cave (Greece). *Quaternary Geochronology, 2*(1–4), 303–308. https://doi.org/10.1016/j.quageo.2006.03.014

van Andel, T. H. (1998). Paleosols, red sediments, and the Old Stone Age in Greece. *Geoarchaeology, 13*(4), 361–390.

van Andel, T. H., & Runnels, C. N. (2005). Karstic wetland dwellers of Middle Palaeolithic Epirus, Greece. *Journal of Field Archaeology, 30*(4), 367–384.

van Wijngaarden, G. J., Merkouri, C., Ligkovanlis, S., Spegi, M., Puijenbroek, F. V., & Versloot, A. (2017). Zakynthos Archaeology Project. The 2015 survey at Skoulikado-Kalimachos. Pharos, 23(2), 1–31. https://doi.org/10.2143/PHA.23.2.3287557

van Wjingaarden, G. J., Kourtessi-Philippakis, G., & Pieters, N. (2013). New archaeological sites and finds on Zakynthos. *Pharos, 1*, 127–159. https://doi.org/10.2143/PHA.19.1.3009293

Vujević, D., & Perhoč, Z. (2024). Musterijenska nalzišta sjeverne Dalmacije: = Mousterian sites in northern Dalmatia. (Kostić, M. Trans.). Zadar: Sveučilište u Zadru.

Zhou, L. P., Van Andel, T. H., & Lang, A. (2000). A luminescence dating study of open-air Palaeolithic sites in western Epirus, Greece. *Journal of Archaeological Science, 27*(7), 609–620. https://doi.org/10.1006/jasc.1999.0484